UC San Diego
UC San Diego Previously Published Works

Title

Three New Species of Deep-Sea Wood-Associated Sea Stars (Asteroidea: Caymanostellidae) from the Eastern Pacific

Permalink

https://escholarship.org/uc/item/1z32s8bd

Journal

Zootaxa, 5536(3)

ISSN

1175-5326

Authors

Shen, Zihui

Koch, Nicolás Mongiardino

Seid, Charlotte A

et al.

Publication Date

2024

DOI

10.11646/zootaxa.5536.3.1

Peer reviewed

Article

Three New Species of Deep-Sea Wood-Associated Sea Stars (Asteroidea: Caymanostellidae) from the Eastern Pacific

ZIHUI SHEN[1], NICOLÁS MONGIARDINO KOCH[1], CHARLOTTE A. SEID[1], EKIN TILIC[2] & GREG W. ROUSE[1*]

[1]*Scripps Institution of Oceanography, University of California San Diego, La Jolla, CA 92093-0202, USA*

✉ *zishen@ucsd.edu;* ⦿ *https://orcid.org/0009-0005-4180-7753*

✉ *nmongiardinokoch@ucsd.edu;* ⦿ *https://orcid.org/0000-0001-6317-5869*

✉ *cseid@ucsd.edu;* ⦿ *https://orcid.org/0000-0002-5307-691X*

✉ *grouse@ucsd.edu;* ⦿ *https://orcid.org/0000-0001-9036-9263*

[2]*Department of Marine Zoology, Senckenberg Research Institute and Natural History Museum,60325 Frankfurt, Germany*

✉ *ekin.tilic@senckenberg.de;* ⦿ *https://orcid.org/0000-0003-0463-322X*

Corresponding author: ✉ *grouse@ucsd.edu*

Abstract

Caymanostellidae is a group of rarely collected and morphologically unusual sea stars that have been exclusively encountered on wood falls in the deep sea. There are currently three genera and seven species described, occurring in the Atlantic, Pacific and Indian Oceans with a depth range between 418 and 6780 m. Three new species are here described from specimens collected from wood falls in multiple localities across the Pacific margin of Costa Rica and near the Gulf of California (Mexico): *Caymanostella scrippscognaticausa* **sp. nov.**, *Caymanostella davidalani* **sp. nov.** and *Caymanostella loresae* **sp. nov.** These records expand the known geographical distribution of caymanostellids and constitute their first report from wood falls found at methane seeps. This study also includes the first descriptions of early-stage juvenile caymanostellids and reveals that traits previously considered useful for diagnosis might represent intraspecific and ontogenetic variability, with important consequences for caymanostellid taxonomy.

Key words: wood fall, methane seep, phylogeny, taxonomy, asteroid, Echinodermata

1. Introduction

Large organic falls, such as wood falls, provide habitats for various organisms in the deep sea. By establishing energy-rich environments in the otherwise nutrient-limited sea floor, they can sustain productive communities of both specialist and opportunistic organisms for relatively long periods, spanning years and even decades (Smith *et al.* 2015). Degradation processes by microbes lead to the development of chemosynthetic microbial communities, facilitating the dispersal of fauna associated with other chemosynthetic environments, and establishing connectivity between methane seeps and hydrothermal vents that would otherwise remain isolated (Bienhold *et al.* 2013; Saeedi *et al.* 2019). It is even hypothesized that decomposing wood falls might have played a role in the origin and early evolution of the fauna endemic to the ocean's chemosynthetic environments (Distel *et al.* 2000). As such, organic falls constitute deep-sea benthic hotspots of biodiversity that can harbor entirely unique communities of organisms and are likely to represent a major source of yet undescribed species. Examples of recently discovered species from wood falls from around the globe include annelids (Barroso *et al.* 2018; Hatch *et al.* 2020; Magalhães *et al.* 2017; Magalhães & Hilliard 2022), nemertines (Hookabe *et al.* 2022; Sagorny *et al.* 2022), molluscs (Duperron *et al.* 2009; Romano *et al.* 2020), crustaceans (Tandberg *et al.* 2013), and echinoderms (Dilman *et al.* 2022; Martin-Cao-Romero *et al.* 2021; Okanishi *et al.* 2020). A few of these species, including some molluscs (Romano *et al.* 2020) and echinoderms (Becker *et al.* 2009; Dilman *et al.* 2022; Mah 2006), represent taxa that have been found exclusively living on wood.

Among living organisms, only a few microbes and fungi can produce enzymes that break down wood cellulose and lignin into more bio-available carbon. Consequently, wood-based diets, or xylophagy, are relatively

---

351

rare among macrofauna. The few organisms capable of feeding exclusively (or predominantly) on wood rely on symbiotic relationships with communities of microorganisms (Becker *et al.* 2009; Romano *et al.* 2020). These organisms can play an important role in altering the wood fall ecosystem. For example, deep-sea wood-boring bivalves, Xylophagaidae Purchon, 1941, can vastly change the structure and biochemical composition of wood fall habitats by exploiting wood that is degraded by endosymbiotic bacteria in their gills (Voight *et al.* 2019; Romano *et al.* 2020; Voight 2015; Bienhold *et al.* 2013). Likewise, the wood-eating sea urchin *Asterechinus elegans* Mortensen, 1942, seems to harbor a microbial community in its guts that assists with wood digestion (Becker *et al.* 2009; Brett 2017). Other notable wood-associated echinoderms with unknown diet include a few rarely encountered groups of sea stars such as *Xyloplax*, Baker, Rowe & Clark, 1986 and Caymanostellidae Belyaev, 1974. Both show unique morphological features compared to other sea stars. While previously known to only occur on wood, a recent study reported the discovery of a new species of *Xyloplax* found on tubeworm bushes at an active hydrothermal vent, which might indicate that their diet is not wood-dependent (Payne *et al.* 2023).

Caymanostellidae Belyaev, 1974 have been found on wood falls from depths ranging from ~414 m to 6780 m in the Pacific, Atlantic and Indian Oceans. The first described species *Caymanostella spinimarginata* Belyaev, 1974, was collected in the Cayman Trench, Caribbean Sea, at around 6740-6780 m (Belyaev, 1974). Currently, there are three genera within Caymanostellidae: *Caymanostella* Belyaev, 1974, including four species; *Belyaevostella* Rowe, 1989, including two species; and the recently described *Crinitostella* Martin-Cao-Romero, Solis-Marin & Bribiesca-Contreras, 2021, which includes a single species. Caymanostellids tend to be flattened and small, with body shapes that vary from pentagonal to subpentagonal to stellate. They have several unique morphological traits that distinguish them from other groups of asteroids, including an abactinal placement of superomarginal plates, the presence of actinal chambers in the inter-radii, bar-shaped adambulacral plates, and an absence of actinal plates (Dilman *et al.* 2022; Rowe 1989).

The four *Caymanostella* species are *C. spinimarginata* Belyaev, 1974, *C. admiranda* Belyaev & Litvinova, 1977, *C. phorcynis* Rowe, 1989, and *C. madagascarensis* Belyaev & Litvinova, 1991. Morphologically, these species can be identified by their unique shape and arrangement of abactinal plates, the shape of abactinal spinelets, the shape of the madreporite (Dilman *et al.* 2022), as well as the position of the gonopores (Dilman *et al.* 2022; Rowe 1989). Due to their small size and probably early developmental stage, known specimens of *C. madagascarensis* lack conspicuous gonopores. A new record of *Caymanostella* from the Kuril-Kamchatka Trench in the West Pacific was recently published by Dilman *et al.* (2022), yet a morphological examination of these specimens and comparison with described species rendered a species-level identification uncertain. Considering this uncertainty and recognizing the possibility that observed morphological differences could reflect ontogeny, Dilman *et al.* (2022) preferred to identify their specimens as *Caymanostella* cf. *spinimarginata*, despite being from different ocean basins and the large geographic distance separating the sampling locality from the type locality of *C. spinimarginata*. Given a lack of available molecular data for *C. spinimarginata* from the type locality in the Caribbean Sea, this assignment cannot yet be tested using molecular approaches.

Belyaevostella can be distinguished from other members of the family by their thick epidermis, superomarginal plates smaller than inferomarginal plates, presence of abactinal papulae, and presence of spicules on the actinal membrane. It further differs from the other genera in terms of the position and shape of the gonopore, and the arrangement of abactinal plates. There are currently two species within *Belyaevostella*: *Belyaevostella hispida* (Aziz & Jangoux 1984) and *Belyaevostella hyugaensis* Fujita, Stampanato & Jangoux, 1994.

Crinitostella was described recently by Martin-Cao-Romero *et al.* (2021) from specimens collected from the Gulf of Mexico. The type and only species is *Crinitostella laguardai* Martin-Cao-Romero, Solis-Marin & Bribiesca-Contreras, 2021, and it constitutes the shallowest record of caymanostellid sea stars (418–427 m). Unlike the other two genera, *Crinitostella* has a more stellate body shape and a unique shape and pattern of abactinal plates. Its abactinal armaments are spiniform rather than granuliform, different from those in *Caymanostella*. It can be further distinguished from *Belyaevostella* based on the absence of abactinal papulae, the absence of spicules on the actinal membrane, and the similar sizes of superomarginal and inferomarginal plates. *Crinitostella* (like *C. madagascarensis*) also has no conspicuous gonopores.

The phylogenetic placement of Caymanostellidae has been debated due to its unique morphological features and rarity. When first described, Caymanostellidae was grouped within Phanerozonia by Belyaev (1974), a heterogeneous group of sea stars containing families currently classified within Paxillosida or Valvatida. Subsequent

authors variously referred the family to Spinulosida (given an overall resemblance with Asterinidae, Aziz & Jangoux, 1984), Velatida (Blake 1987; Smith 1988), and Valvatida (Rowe 1988; Rowe 1989). A possible relationship between Caymanostellidae and Xyloplacidae was also suggested, as both lineages were known to be wood-associated and shared an overall resemblance (Belyaev 1990; Smith 1988; Gale 2011). Subsequent molecular phylogenetic analyses showed that *Xyloplax* did not form a clade with Caymanostellidae (Janies *et al.* 2011; Mah & Blake 2012; Martin-Cao-Romero *et al.* 2021; Dilman *et al.* 2022), supporting the conclusion that similarities between the two were the product of adaptation to similar environments. While *Xyloplax* is today generally placed within Velatida (Linchangco *et al.* 2017; Payne *et al.* 2023), Caymanostellidae is generally recovered as a member of Valvatida (Martin-Cao-Romero *et al.* 2021; Dilman *et al.* 2022; Mah & Blake 2012).

Accurate identification of caymanostellid specimens is complicated by a lack of understanding of how their morphology varies through ontogeny. Belyaev (1974) found that characters such as the number and size of plates, the density of abactinal armaments, and the spine length can vary with body size among specimens of *Caymanostella spinimarginata*. Similarly, Rowe (1989) noticed some features that might vary with body size in *Belyaevostella hispida*, including skin thickness and the size and shape of superomarginal plates. Dilman *et al.* (2022) also highlighted potential ontogenetic differences among specimens of *Caymanostella* and suggested the madreporite could vary from slit-like in early adult stages to complex with branching grooves in larger adults. However, all reported specimens to date have been interpreted as adults, and no records exist of earlier life stages (larvae or juveniles). As discussed in Dilman *et al.* (2022), it has been speculated that *Caymanostella* are direct developers based on the large size of eggs, as well as the presence of inter-radial actinal chambers hypothesized to be used for brooding. There is currently no direct evidence of this.

Molecular data for Caymanostellidae has been limited to date. The few past studies that produced molecular phylogenies relied on different molecular markers and were unable to include data for all members of the clade. There are no published sequences for *Caymanostella admiranda*, *C. phorcynis*, *C. madagascarensis*, or any members of *Belyaevostella*.

Expeditions to the Pacific margin of Costa Rica and Gulf of California, Mexico have resulted in the collection of new specimens of caymanostellid sea stars, including several specimens of various sizes discovered on wood falls located on a seamount and methane seeps. Wood deployment experiments in this area also resulted in the collection of juvenile individuals. These specimens (whose publicly accessible localities were also included in Fig. 1 of Dilman *et al.* (2022)) represent the first records of caymanostellids in these localities. Here, we leverage molecular and morphological approaches to support the placement of these specimens within three new species of caymanostellid sea stars.

2. Materials and Methods

2.1 Sample collection and preservation

During cruises to the Pacific margin of Costa Rica undertaken between 2009 and 2018 by R/V *Atlantis*, HOV *Alvin* collected caymanostellid specimens from wood falls at several localities (Figs 1, 2A–E), including active methane seep sites at Mound 11, Mound 12, and Jaco Scar, as well as the non-methane-seep site Seamount 2 (Fig. 1B). The samples contained both juvenile and mature individuals spanning a range of body sizes, and the collection depth ranged from 974 to 1887 m. Specimen collection was performed under permits INCOPESCA-CPI-003-12-2018, R-070-2018-OT-CONAGEBIO, SINAC-CUSBSE-PI-R-032-2018, and SINAC-SE-CUS-PI-R-035-2017. Collection data is listed in Table 1. Most specimens were photographed live in the field with a Leica S8Apo stereo microscope + Canon Powershot G9 camera or with a Leica MZ9.5 stereo microscope + either a Canon Powershot G9 or a Canon EOS Rebel T6S camera. Additional pictures were taken post-preservation with a Leica MZ12.5 stereo microscope and Canon EOS Rebel T6s or 850D camera. Samples were fixed with 95% ethanol, RNAlater (Ambion, Inc., now Thermo Fisher Scientific Inc., Waltham, MA, USA), Prefer (glyoxal fixative, Anatech, Battle Creek, MI, USA), glutaraldehyde-osmium tetroxide, or seawater-buffered formalin in the field, and were preserved in 50% or 95% ethanol and deposited at the Benthic Invertebrate Collection at Scripps Institution of Oceanography (SIO-BIC), La Jolla, California, USA, the Museo de Zoología, Universidad de Costa Rica (MZUCR), San José, Costa Rica or the Marine Invertebrates II section of the Senckenberg Research Institute and Natural History Museum (SMF), Frankfurt, Germany.
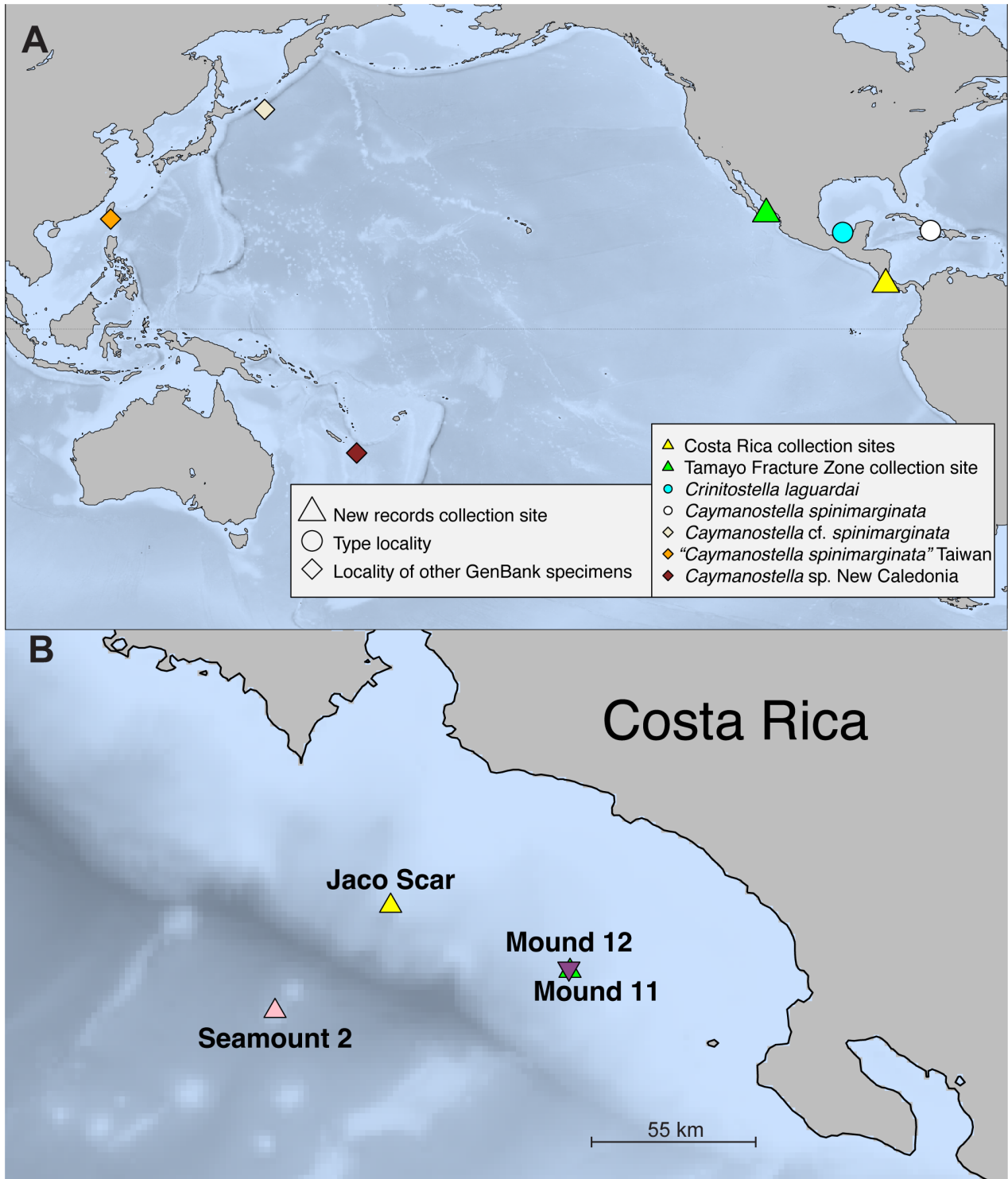
FIGURE 1. Geographic distribution of selected caymanostellids, including records for both novel and previously known specimens. A—Localities of type specimens and taxa with available molecular and locality data; B—Detailed collection sites for new Costa Rica specimens, note that Jaco Scar, Mound 11 and Mound 12 are active methane seep sites.

TABLE 1. Biogeographic information and GenBank accession numbers of taxa (where applicable) and specimens used in this study. Locality information is only included for Caymanostellidae specimens. *Holotype. **Synonymized as *Caymanostella*.

Taxonomy	Species/other names used	Voucher	Locality	COI	16S	H3	References
Valvatida, Caymanostellidae	*Caymanostella scrippscognaticausa* **sp. nov.**	SIO-BIC E11441*	Mound 11, Costa Rica	PP627110	PP572462	PP658046	This study
		SIO-BIC E7289	Mound 11, Costa Rica	PP627119			This study
		SIO-BIC E7290A, C,D,E/ MZUCR-ECH2402, F	Mound 11, Costa Rica	PP627111-15			This study
		SIO-BIC E4383	Mound 12, Costa Rica	PP627105			This study
		SIO-BIC E4384	Mound 12, Costa Rica				This study
		SIO-BIC E11442	Mound 12, Costa Rica	PP627106			This study
		SIO-BIC E4549A, B/SMF 6939, D, E, G	Mound 12, Costa Rica	PP627120-2323			This study
		SMF 6938	Mound 12, Costa Rica				This study
		SIO-BIC E11221A, B	Mound 12, Costa Rica	PP627116-17			This study
		SIO-BIC E7075A, B,D	Mound 12, Costa Rica	PP627107 -09			This study
		SIO-BIC E7228	Mound 12, Costa Rica	PP627118			This study
		SIO-BIC E4403	Jaco Scar, Costa Rica	PP627104			This study
	Caymanostella davidalani **sp. nov.**	SIO-BIC E7101*	Seamount 2, Costa Rica	PP627124	PP572463	PP658047	This study
		MZUCR-ECH2403	Mound 12, Costa Rica	PP627125			This study
		SIO-BIC E7226	Jaco Scar, Costa Rica	PP627128		PP658050	This study
		SIO-BIC E7238	Jaco Scar, Costa Rica	PP627127		PP658049	This study
		SIO-BIC E7242	Jaco Scar, Costa Rica	PP627126		PP658048	This study
	Caymanostella loresae **sp. nov.**	ICML-EMU-13880*	Gulf of California, Mexico				This study
		SIO-BIC E11393A/SMF 6940, B, C, D	Gulf of California, Mexico				This study
		USNM1487403	Gulf of California, Mexico	PP627129	PP572464	PP658051	This study
	Caymanostella cf. *spinimarginata* Belyaev, 1974	CsSO250-9-1	Kuril-Kamchatka Trench, Japan	MW591935	MW591921	MW591943	Dilman *et al.* (2022)

TABLE 1 (Continued)

Taxonomy	Species/other names used	Voucher	Locality	COI	16S	H3	References
		CsSO250-9-2	Kuril-Kamchatka Trench, Japan	MW591936	MW591922	MW591944	Dilman *et al.* (2022)
		CsSO250-9-3	Kuril-Kamchatka Trench, Japan	MW591937	MW591923	MW591945	Dilman *et al.* (2022)
	Caymanostella laguardai (Martin-Cao-Romero, Solis-Marin & Bribiesca-Contreras, 2021), n. comb.**	NHMUK:2021.1	Gulf of Mexico, Mexico		MW556266	MW556265	Martin-Cao-Romero *et al.* (2021)
	'Caymanostella spinimarginata' Taiwan	MNHNP EcAh 5244	Taiwan, China	JQ918260	JQ918328	JQ918212	Foltz and Fatland (2012) unpublished
	Caymanostella sp.	MNHNP EcAs 12356	New Caledonia			EU707760	Foltz *et al.* (2008) unpublished
	Caymanostella sp.	FMNH 5167	Oregon, USA		DQ297082		Janies *et al.* (2011)
Valvatida, Ophidiasteridae	*Leiaster glaber* Peters, 1852	Ech 247		EU869940	EU722945	EU707748	Ward *et al.* (2008)
Valvatida, Odontasteridae	*Diplodontias miliaris* Gray, 1847	AMCC 113392		DQ380240	DQ297078	DQ676900	Janies *et al.* (2011)
	Eurygonias hylacanthus Farquhar, 1913	AMCC 114324		DQ380238	DQ297089	DQ676908	Janies *et al.* (2011)
	Odontaster validus Koehler, 1906	AMCC 113405			DQ297101	DQ676918	Janies *et al.* (2011)
Valvatida, Solasteridae	*Crossaster papposus* Linnaeus, 1767	AMCC 113349		AF217383	DQ297084	DQ676904	Janies *et al.* (2011)
	Solaster stimpsoni Verrill, 1880	AMCC 113400		AF217382	DQ297113	DQ676930	Janies *et al.* (2011)
Velatida, Korethrasteridae	*Peribolaster folliculatus* Sladen, 1889	CASIZ 163123		JQ918217	EU072955	EU707668	Mah and Foltz (2011a)
Velatida, Xyloplacidae	*Xyloplax janetae* Mah, 2006	FMNH 12460		DQ377828	DQ777080		Janies *et al.* (2011)
Velatida, Pterasteridae	*Hymenaster pellucidus* Thomson, 1873	AMCC 113310/ HpelPS128-44-1		MW591941	MW591927	MW591949	Dilman *et al.* (2022)
	Pteraster militaris O.F. Müller, 1776	CASIZ 174315/ AMCC 113311 /PtmilAMK54-4960-1		MW591942	EU722967	MW591950	Dilman *et al.* (2022); Mah and Foltz (2011b)

During a 2003 cruise to the Gulf of California by R/V *Western Flyer*, caymanostellid specimens were collected by ROV *Tiburon* from a single wood fall at the Tamayo Fracture Zone off western Mexico near the Gulf of California at 3054 m depth (Figs 1A, 2F). Collected specimens were all adults. Five of these were fixed in formalin, preserved in 50% ethanol and deposited at SIO-BIC, SMF, and the Colección Regional de Invertebrados Marinos, Estación Mazatlán UNAM, Instituto de Ciencias del Mar y Limnología, Universidad Nacional Autónoma de México (ICML-EMU), Mazatlán, Sinaloa, Mexico. One additional specimen was fixed and preserved in 95% ethanol and deposited at the Smithsonian National Museum of Natural History (USNM), Washington, D.C., USA. Pictures of preserved specimens were taken with a Leica MZ12.5 stereo microscope and Canon EOS Rebel T6S or 850D camera. All institutional catalog numbers can be found in Table 1 and the formal descriptions.
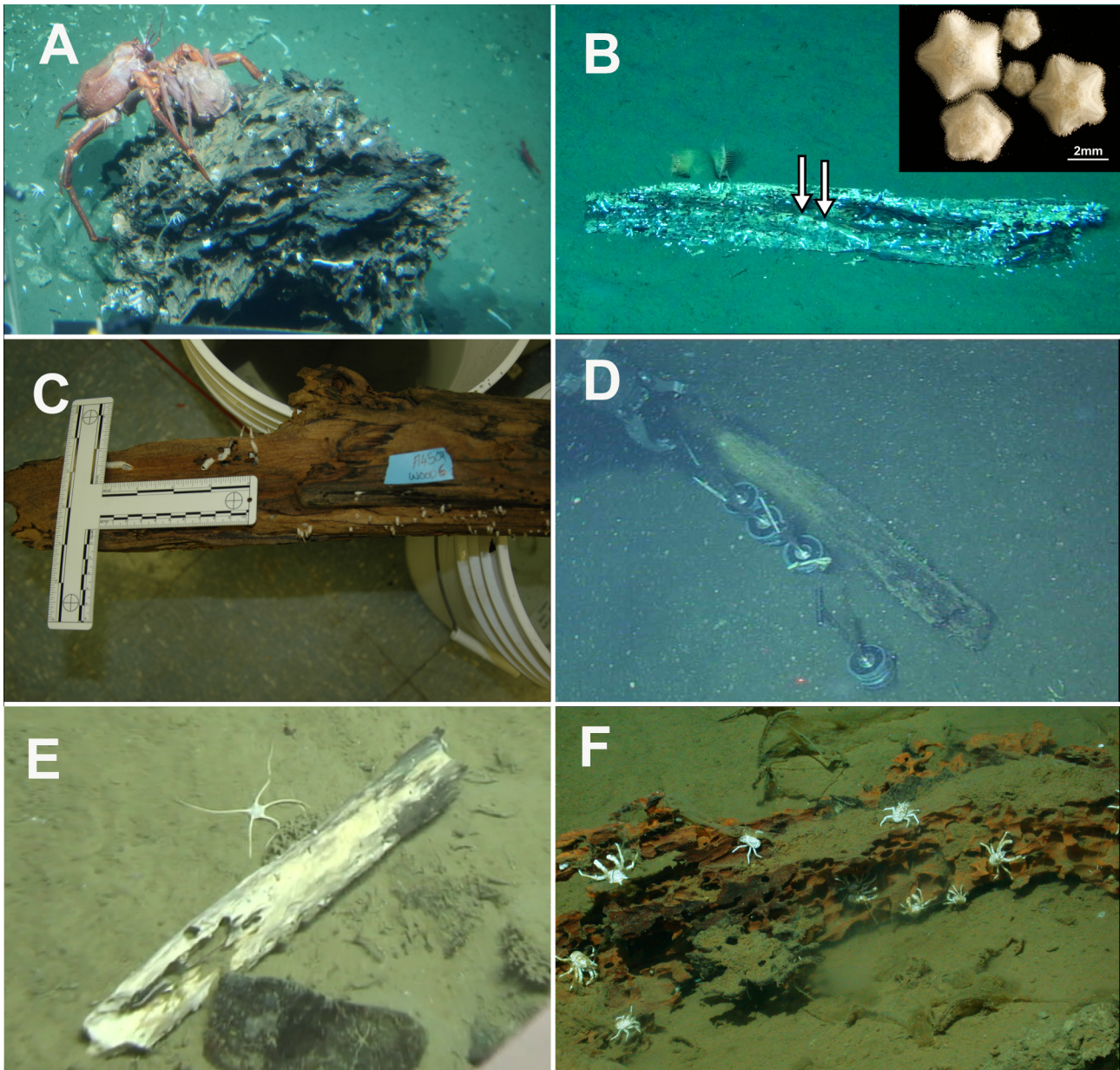
FIGURE 2. Examples of collection sites yielding new specimens. A—Wood at Mound 11, Pacific margin of Costa Rica, that yielded several specimens of *Caymanostella scrippscognaticausa* **sp. nov.**, including the holotype (SIO-BIC E11441), HOV *Alvin* dive 4988; B—Wood at Mound 12, Pacific margin of Costa Rica, that yielded specimens of *Caymanostella scrippscognaticausa* **sp. nov.** (SIO-BIC E7075) and *Caymanostella davidalani* **sp. nov.** (MZUCR ECH2403), two visible specimens are indicated with arrows, HOV *Alvin* dive 4922; C—Wood collected at Jaco Scar, Pacific margin of Costa Rica, HOV *Alvin* dive 4509; D—Wood being collected by HOV *Alvin* at Jaco Scar, Pacific margin of Costa Rica, HOV *Alvin* dive 4509; E—Wood at Seamount 2, Pacific margin of Costa Rica, that yielded the holotype of *Caymanostella davidalani* **sp. nov.** (SIO-BIC E7101), HOV *Alvin* dive 4926; F—Wood at Tamayo Fracture Zone, Gulf of California, Mexico, that yielded specimens of *Caymanostella loresae* **sp. nov.**, including the holotype (ICML-EMU-13880), ROV *Tiburon* dive 553, © MBARI 2003.

2.2 DNA extraction, amplification, and sequencing

DNA extraction was performed on selected specimens using the Zymo Research DNA-Tissue Miniprep or Microprep kits (Zymo Research, Irvine, CA, USA) based on the manufacturer's protocols. Mitochondrial cytochrome c oxidase subunit I (COI) DNA sequences were obtained from a total of 26 caymanostellid specimens. To aid comparison with *Crinitostella laguardai* (for which no COI sequences are available; see Table 1), mitochondrial 16S rRNA (16S)

and nuclear histone H3 (H3) sequences were obtained from representatives of each of the three new species. The primers used for amplification are listed in Table 2. For each specimen, a polymerase chain reaction (PCR) master mix was created using 12.5 µl of Taq DNA polymerase, 1 µl of corresponding forward and reverse primer stocks, 8.5 µl of ddH$_2$0, and 2 µl of eluted DNA extraction. COI was amplified following the PCR temperature reaction profile: Initial denaturation at 95 ºC /2min, followed by 35 cycles of denaturation at 95 ºC /30s, annealing at 48 ºC /30s, elongation at 72 ºC /45s, and final extension at 72 ºC /10min. 16S was amplified following the temperature reaction profile: Initial denaturation at 95 ºC /3min, followed by 40 cycles of denaturation at 95 ºC /40s, annealing at 50 ºC /40s, elongation at 72 ºC /50s, and final extension at 72 ºC /5min. H3 was amplified following the temperature reaction profile: Initial denaturation at 95 ºC /3min, followed by 40 cycles of denaturation at 95 ºC /30s, annealing at 53 ºC /54s, elongation at 72 ºC /45s, and final extension at 72 ºC /5min.

TABLE 2. PCR primers used for each gene.

Gene	Primer Name	Primer sequence 5'-3'	References
COI	COIeF	ATA ATG ATA GGA GGR TTT GG	Arndt *et al.* 1996
COI	COIeR	GCT CGT GTR TCT ACR TCC AT	Arndt *et al.* 1996
16S	16sar-L	CGCCTGTTTATCAAAAACAT	Palumbi 1996
16S	16sbr-H	CCGGTCTGAACTCAGATCACGT	Palumbi 1996
H3	H3F	ATGGCTCGTACCAAGCAGACVGC	Colgan *et al.* 2003
H3	H3R	ATATCCTTRGGCATRATRGTGAC	Colgan *et al.* 2003

PCR products were purified with ExoSAP-IT (USB Corporation, OH, USA) and Sanger sequencing was performed by Eurofins Genomics (Louisville, KY, USA). Forward and reverse sequences were *de novo* assembled on Geneious Prime 2023.2.2 (http://www.geneious.com) under default settings. Consensus reads were generated after removing base pairs of poor quality and manually resolving most ambiguities. BLAST (Altschul *et al.* 1990) searches against the NCBI GenBank repository were conducted to check the direction and confirm the identity of each consensus read. All sequences generated in this study are deposited in GenBank; accession numbers and other specimen details are in Table 1.

2.3 Sequence analysis and phylogenetic inference

A maximum likelihood (ML) analysis was performed on the available COI data for Caymanostellidae and the newly generated sequences with RAxML-NG v. 1.1.0 (Kozlov, 2019) using the RAxML GUI v. 2.0.10 (Edler *et al.,* 2021) and the model GTR+I+G. For the multi-locus analysis, available COI, 16S, and H3 sequences of *Caymanostella* and *Crinitostella* on GenBank (Table 1) were downloaded and used along with the new sequences generated here to perform a more comprehensive phylogenetic analysis of Caymanostellidae. A diverse set of outgroup terminals was sampled from across the orders Valvatida and Velatida, following the recent phylogenetic studies of Martin-Cao-Romero *et al.* (2021) and Dilman *et al.* (2022). A character matrix was created with Mesquite v. 3.70 (Maddison and Maddison, 2023), and sequences were aligned with MAFFT 7 using the Q-INS-I setting (Katoh and Standley, 2013).

For phylogenetic inference, a concatenated alignment of the three loci was generated using Sequence Matrix (Vaidya *et al.,* 2011), including sequences for all loci obtained from a representative of each of the three new species. The aligned concatenated dataset had a total of 2,318 nucleotide positions. The ML analysis was performed with RAxML-NG v. 1.1.0 using the RAxML GUI v. 2.0.10 with the dataset was partitioned by gene, and optimal models chosen with ModelTest-NG (Darriba *et al.*, 2020) as follows: GTR+I+G for COI, TPM3uf+I+G for 16S, and TVM+I+G for H3. Ten ML searches were performed, and node support values were estimated using 1,000 bootstrap replicates.

Uncorrected and model corrected (COI: TIM2+I; 16S: GTR+G) pairwise distances for COI and 16S sequences of caymanostellids were computed with PAUP*(Swofford, 2003). Optimal models were chosen with ModelTest-NG (Darriba *et al*., 2020). A 16S pairwise distance analysis of caymanostellids was included due to the lack of COI sequences for *Crinitostella*. COI haplotype networks were created with PopART v.1.7 (Leigh and Bryant 2015) using the TCS network option (Clement *et al.* 2000).

2.4 Morphological analysis

Specimens were examined using a Leica MZ12.5 stereo microscope and photographed as previously mentioned. Several drops of 12% bleach were added onto selected specimens to dissolve tissues and separate spines from plates for detailed analysis. Three specimens (SMF 6939, SMF 6938, SMF 6940) were stained in 1% osmium tetroxide for 90 minutes and used for micro-computed tomography (μCT) analysis with a Werth Tomoscope® XS Plus 200 scanner. Renderings were generated using the visualization software Drishti v3.1 (Limaye, 2012). Scan parameters for SMF 6939 were: voltage 85kV, generator current 188 μA, generator power 16 W, voxel size 5.65 μm, exposure time 500 ms and a total of 4200 projections (3 projections were averaged). Scan parameters for SMF 6938 were: voltage 85kV, generator current 59 μA, generator power 5 W, voxel size 2.46 μm, exposure time 1500 ms and a total of 4100 Projections (2 projections were averaged). Scan parameters for SMF 6940 were: voltage 100kV, generator current 110 μA, generator power 11 W, voxel size 8.78 μm, exposure time 666 ms, and a total of 3759 Projections (3 projections were averaged). Representatives of each species were also chosen for Scanning Electron Microscopy (SEM) analysis, including the holotype of *Caymanostella davidalani* **sp. nov.**, paratype specimens, and disarticulated spine material of all novel species (see Materials Examined). Samples were rinsed in ethanol, air dried and mounted on aluminum stubs using double-sided carbon adhesive tabs and tape. Each sample was then coated with gold-palladium using a metal sputter coater before being examined under a Zeiss EVO10 scanning electron microscope operating at 20 kV.

3. Results

3.1 Phylogeny

Initial phylogenetic analyses employing COI data (Fig. 3A) showed that the new specimens formed three clades, two with multiple members and one represented by a singleton. All three clades were divergent from the publicly available caymanostellid COI sequences. Results from the ML analysis of the COI (Fig. 3A), concatenated dataset (Fig. 3B) and estimation of molecular distances all supported the recognition of two new species from the Pacific margin of Costa Rica and one new species from the opening of the Gulf of California (Mexico), each in a well-supported clade: *Caymanostella scrippscognaticausa* **sp. nov.**, found on wood falls near methane seeps on Mound 11, Mound 12, and Jaco Scar (Costa Rica); *Caymanostella davidalani* **sp. nov.**, found on wood falls at Seamount 2 and near methane seeps on Mound 12 and Jaco Scar (Costa Rica); and *Caymanostella loresae* **sp. nov.**, found on wood falls at the Tamayo Fracture Zone (Mexico) (Fig. 3A, B).

The overall tree topology generally matched the results of other recent publications (Martin-Cao-Romero *et al.* 2021; Dilman *et al.* 2022). *Caymanostella scrippscognaticausa* **sp. nov.** was recovered as the sister group to *Crinitostella laguardai*, and this clade resolved in turn as sister to *Caymanostella davidalani* **sp. nov.**, with both nodes showing high support. These species were sister to *Caymanostella* cf. *spinimarginata*, forming a clade sister to *Caymanostella loresae* **sp. nov.**, again with high support. Except for an apparently misidentified specimen of *Caymanostella* from New Caledonia, all other caymanostellid sequences form a well-supported clade (Fig. 3). These species all inhabit the Pacific Ocean, with the sole exception of *Crinitostella laguardai*, which is from the Gulf of Mexico (Figs 1A). The nesting of *Crinitostella laguardai* within *Caymanostella* suggests they should be treated as synonyms and since *Crinitostella* is the younger name we treat it hereafter as *Caymanostella laguardai* (see below).
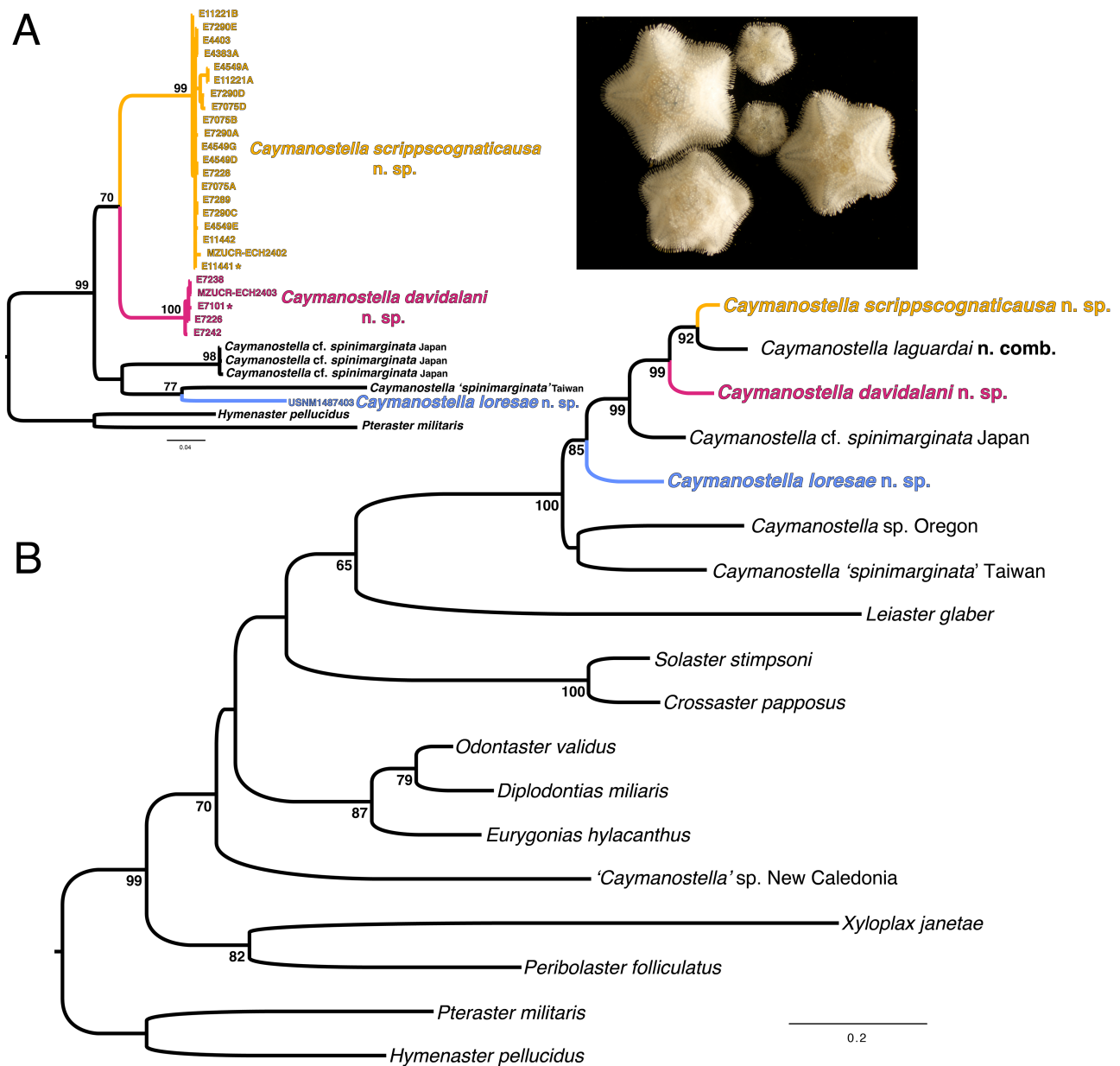
FIGURE 3. Phylogenetic analyses. A—Maximum Likelihood analysis of mitochondrial COI of available *Caymanostella* sequences from GenBank, plus the newly generated sequences for this study. Sequences for *Caymanostella scrippscognaticausa* **sp. nov.** and *C. davidalani* **sp. nov.** holotypes are indicated by a *. Numbers on nodes represent ML bootstrap values. The three new species are highlighted in bold and color. B—Maximum Likelihood tree generated from concatenation of mitochondrial (COI and 16S) and nuclear (H3) genes. Numbers on nodes represent ML bootstrap values. The three new species are highlighted in bold and color. Sequences for *Caymanostella scrippscognaticausa* **sp. nov.** and *C. davidalani* **sp. nov.** are from the respective holotypes, except for the H3 sequence for *C. davidalani* **sp. nov.** which is from a paratype (SIO-BIC E7242). Sequences for *C. loresae* **sp. nov.** are from paratype USNM 1487403. *Crinitostella* is synonymized as *Caymanostella* (see Discussion).

3.2 Species delimitation and haplotype networks

Intraspecific COI distances (Table 3) were low among specimens of *Caymanostella scrippscognaticausa* **sp. nov.** and *Caymanostella davidalani* **sp. nov.** (maximum uncorrected distances of 1.8% and 1.0%, respectively). Minimum interspecific COI distances from *Caymanostella* cf. *spinimarginata* were much higher (minimum uncorrected distance of 13.7% for *C. scrippscognaticausa* **sp. nov.**, 14.1% for *C. davidalani* **sp. nov.**, and 14.3% for *C. loresae* **sp. nov.**). The 16S pairwise distances showed a large divergence between the new species and *C.*

laguardai (uncorrected distance of 6.4% for *C. scrippscognaticausa* **sp. nov.**, 8.6% for *C. davidalani* **sp. nov.**, and 14.6% for *C. loresae* **sp. nov.**, Table 4).

TABLE 3. Pairwise distance for COI of species where data is available. Values shown are uncorrected followed by model corrected (TIM2+I+G) pairwise distances. Minimum interspecific pairwise distances are shown in off-diagonal cells; maximum intraspecific pairwise distances are shown in cells across the diagonal. Maximum intraspecific pairwise distances of new species are highlighted in bold.

		1	2	3	4
1.	*Caymanostella* cf. *spinimarginata*	0.2–0.3%	13.7–22%	14.1–22.8%	14.3–24.3%
2.	*Caymanostella scrippscognaticausa* **sp. nov.**		**1.8–1.9%**	10.5–14.4%	17.5–31.2%
3.	*Caymanostella davidalani* **sp. nov.**			**1.0–1.0%**	15.9–26.6%
4.	*Caymanostella loresae* **sp. nov.**				-

TABLE 4. Pairwise distance for 16S of species where data is available. Values shown are uncorrected followed by model corrected (GTR+G) pairwise distances. Minimum interspecific pairwise distances are shown in off-diagonal cells; maximum intraspecific pairwise distances are shown in cells across the diagonal. *Crinitostella* is synonymized as *Caymanostella*.

		1	2	3	4	5
1.	*Caymanostella* cf. *spinimarginata*	1.0%–1.0%	10.2%–19.2%	6.1%–9.4%	6.4%–9.5%	10.3%–20.7%
2.	*Caymanostella laguardai* n. comb.			6.4%–9.4%	8.6%–14.2%	14.6%–41.8%
3.	*Caymanostella scrippscognaticausa* **sp. nov.**				5.6%–7.4%	12.9%–32.9%
4.	*Caymanostella davidalani* **sp. nov.**					11.3%–25.5%
5.	*Caymanostella loresae* **sp. nov.**					

The COI haplotype network of *Caymanostella scrippscognaticausa* **sp. nov.** revealed the presence of 13 different haplotypes over a geographical range of approximately 62 km, from Jaco Scar to Mound 11 and Mound 12 (Fig. 4A). There was no evidence of genetic isolation between these populations, and one haplotype was present in all three localities. Sampling depth was not included in this network because collection depth was not recorded for the Jaco Scar individual. The COI haplotype network of *Caymanostella davidalani* **sp. nov.** (Fig. 4B, C) also did not show strong evidence of population structure across either geographic range or depth.

3.3 Taxonomy

Caymanostellidae Belyaev, 1974

Type genus. *Caymanostella* Belyaev, 1974

Diagnosis (emended). Body pentagonal to stellate in outline. Abactinal side slightly convex. Abactinal plates imbricate, polygonal to oval or circular shaped. Superomarginal plates located on the abactinal side. Inferomarginal plates rectangular to bar-shaped, delimiting body margin, and either similar in size or larger than superomarginal plates. Actinal plates absent. Two rows of tube feet. Adambulacral plates bar shaped, extending between ambulacral and inferomarginal plates. Five interradial chambers, each containing one pair of gonads, visible through a thin membrane on the actinal side. One pair of gonopores per interradius, associated with the two proximal-most superomarginal plates.

Remarks. The diagnosis of Caymanostellidae is emended from Rowe (1989) to accommodate the new species described in this work, in addition to *C. laguardai* from the Gulf of Mexico. Characters described are shared among adult specimens. Also, the terms actinal and abactinal are used instead of oral and aboral, consistent with current practice. Rowe (1989) noted some shared characters between Caymanostellidae and the Lower Jurassic taxa *Protremaster*, which is currently placed in Asterinidae.
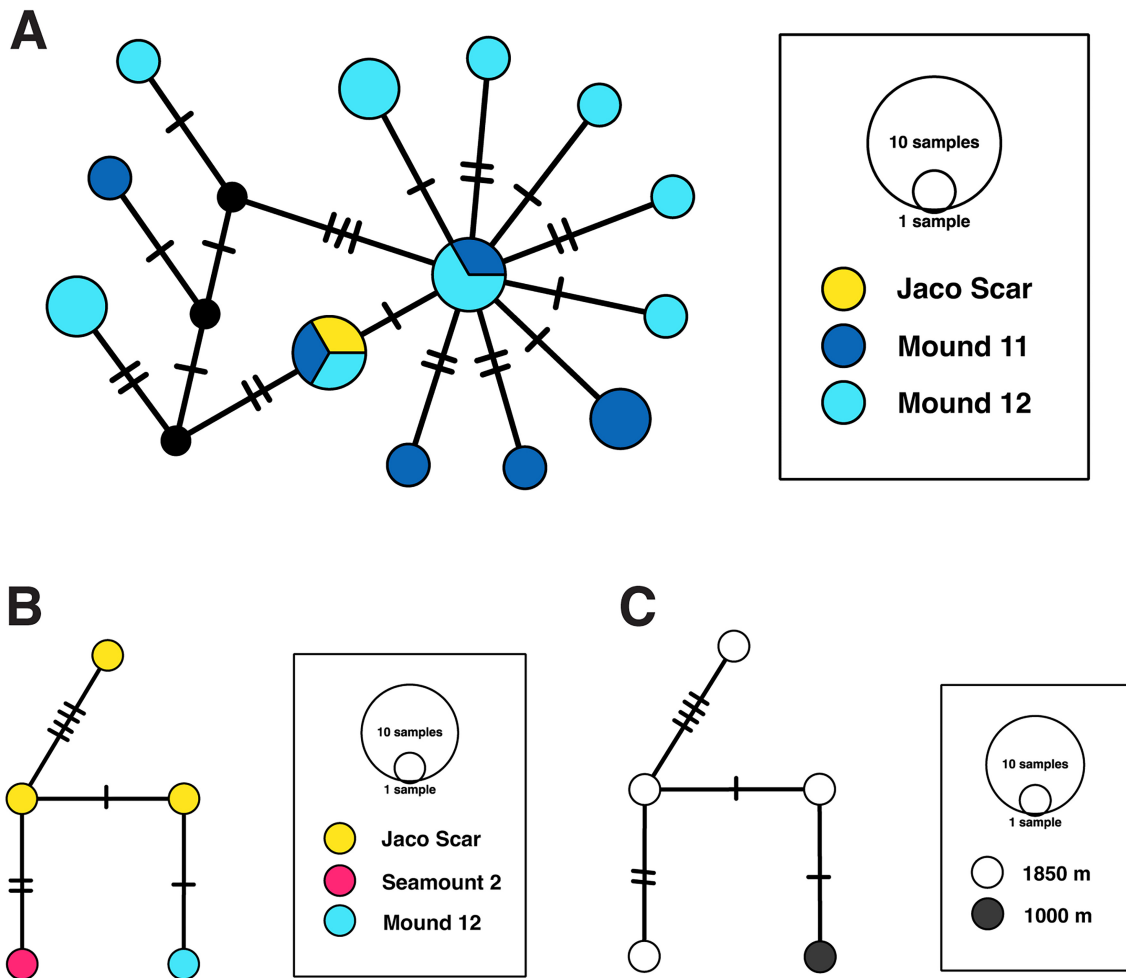
FIGURE 4. COI haplotype networks. A—*Caymanostella scrippscognaticausa* **sp. nov.** locality network; B—*Caymanostella davidalani* **sp. nov.** locality network; C—*Caymanostella davidalani* **sp. nov.** depth network.

Caymanostella Belyaev, 1974

Type species. *Caymanostella spinimarginata* Belyaev, 1974

Diagnosis (emended). Adult body pentagonal to stellate in outline with thin or thick epidermis. Abactinal plates polygonal to oval or circular shaped. Inferomarginals similar in size to the adjoining superomarginals or larger. Granuliform to spiniform abactinal armaments. Club-shaped fringe spines on edges of inferomarginal plates. Gonopores either in notches at the proximal margin of two proximal-most superomarginal plates or piercing through the plates. Papulae absent. Actinal membrane with no spicules.

Remarks. Notable features of *Caymanostella* include granuliform to spiniform abactinal armament, and their gonopores are either located in notches of the proximal-most superomarginal plates, or pierce through them (Dilman *et al.* 2022; Rowe, 1989). The diagnosis of *Caymanostella* is emended from Rowe (1989) to accommodate two new species from the Pacific margin of Costa Rica, *Caymanostella scrippscognaticausa* **sp. nov.** and *Caymanostella davidalani* **sp. nov.**, as well as one new species from the Gulf of California, *Caymanostella loresae* **sp. nov.**, based on characters shared among adult specimens. Molecular data of the type specimen or from the type locality is needed to further evaluate the monophyly and taxonomy of *Caymanostella*.

Caymanostella scrippscognaticausa sp. nov.
Figures 5–10

Alvarado *et al.* (2022) Table 1, as *Belyaevostella* sp., *Caymanostella* sp.

Diagnosis. Adult body stellate. Juveniles pentagonal to subpentagonal. Abactinal plates oval to polygonal shaped with curved margin. Abactinal armament spiniform and sparsely distributed. Central disc plates of various sizes but similar shapes and imbricating in irregular cycles. One row of dorsal-lateral plates on each side of a row of carinal plates which are less discernible closer to arm base. Terminal plate square-shaped. Each inferomarginal plate larger than adjoining superomarginal plate. Gonopores visible, located in notches at the radial margin of the proximal-most superomarginal plates. Madreporite single pore or slit to complex grooves. Wide, robust adambulacral spines.

Materials Examined. Holotype: SIO-BIC E11441, on wood at Mound 11, Costa Rica, 8.9221°N, 84.3045°W, 1010 m depth, November 3, 2018, HOV *Alvin* dive 4988, collectors Victoria Orphan and Hang Yu [GenBank: COI = PP627110; 16S = PP572462; H3 = PP658046]. **Paratypes:** SIO-BIC E7290A (prepared for SEM), E7290C (prepared for SEM), E7290D (prepared for SEM), SIO-BIC E7290F, SIO-BIC E7289, MZUCR ECH2402, same collection data as holotype; SIO-BIC E4383, SIO-BIC E11442, on wood at Mound 12, Costa Rica, 8.9297°N, 84.3115°W, 990 m depth, February 24, 2009, HOV *Alvin* dive 4503, collectors Erik Cordes and Jen Gonzalez; SIO-BIC E4549A (prepared for SEM), SMF 6939 (fixed glutaraldehyde-OsO$_4$, prepared for μCT), SIO-BIC E4549D (prepared for SEM), SIO-BIC E4549E, SIO-BIC E4549G, SIO-BIC E11221A, SIO-BIC E11221B, on wood at Mound 12, Costa Rica, 8.9306°N, 84.3124°W, 996 m depth, January 8, 2010, HOV *Alvin* dive 4587, collectors Victoria Orphan and Maria Teresa Aguado; E7075A (prepared for SEM), E7075B (prepared for SEM), SIO-BIC E7075D, on wood at Mound 12, Costa Rica, 8.9325°N, 84.3074°W, 1002 m depth, June 5, 2017, HOV *Alvin* dive 4922, collectors Jen Le and Chris Roman. **Other materials:** SIO-BIC E4384 (fixed in Prefer), same collection data as SIO-BIC E4383; E7228 (specimen completely used up for DNA extraction; COI = PP627118), from bone and wood deployment at Mound 12, Costa Rica, 8.9300°N, 84.3117°W, 992 m depth, October 20, 2018, HOV *Alvin* dive 4974, collectors Lisa Levin and Kyle Metcalfe; SIO-BIC E4403 (specimen completely used up for DNA extraction; COI = PP627104), substrate not recorded, at Jaco Scar, Costa Rica, 9.1262°N, 84.8384°W, 974–1856 m, exact depth not recorded, Mar 3, 2009, HOV *Alvin* dive 4509, collectors Elena Perez and Jake Bailey.

Description. Adult body stellate (Range of adult specimens: R = 2.88–6.85 mm, r = 2.33–4.65 mm, R/r = 1.21–1.77; Holotype: R = 5.85 mm, r = 4.15 mm, R/r = 1.41, bent, so measurement may not be accurate). Thin epidermis covers abactinal surface. Epidermis thicker on actinal surface. Abactinal plates oval or irregularly polygonal with curved edges, wider than long, and imbricated so that distal edge of each plate is overlapped by proximal edge of one or more plates. Central disc plates more irregular in shape and sizes than arm plates and appear thick, causing abactinal surface to look uneven due to imbrication. Central disc plates imbricated more irregularly than arm plates. Five primary inter-radial plates (one bearing the madreporite) appear much larger than other abactinal plates and irregularly polygonal. Madreporite of holotype with multiple branching grooves (Figs 5H, 10A). A single row of dorsal-lateral plates on each side of a single row of carinal plates (Figs 6E, 8A) on each arm; rows of plates tend to become less discernible closer to the central disc. Some individuals have a second row of dorsal-lateral plates at arm base, which is more discernable in large specimens that have more plates. The row of carinal plates leads to a square-shaped terminal plate at tip of the arm with a central pore (Figs 6E, 8A). Each central disc plate bears around 12 or less abactinal armaments, sparsely distributed (~20/mm^2), short (0.08–0.2 mm) and spiniform. Abactinal spinelets consist of rounded, wide and robust base and stem with longitudinal ridges leading to a slightly expanded and thorny crown (Fig. 8E, F). Other abactinal plates bear spines of a similar shape. Each terminal plate has 4–5 elongated abactinal spines (0.1–2.5 mm), and 2–3 club shaped fringe spines (0.4–0.5 mm).

Along each side of the arm there are parallel rows of superomarginal plates and inferomarginal plates, more pentagonal than the abactinal plates. Each row has the same number of plates (adults 8–13; 9 in holotype) from inter-radius to arm tip, imbricating radially. Both rows uniform in shape except for proximal-most superomarginal plate. Each inferomarginal plate slightly more elongated and larger in size compared to adjoining superomarginal plate. First and/or second proximal-most superomarginal and inferomarginal plates are largest, size of plates decreases towards arm tip. Proximal-most superomarginal plate the most-oval shaped, wider than long. Marginal plates and other abactinal arm plates form a cohesive and convex abactinal surface. Gonopores conspicuous in interradius in holotype (Fig. 5E). Each of two gonopores on interradius in a notch associated with proximal-radial margin of
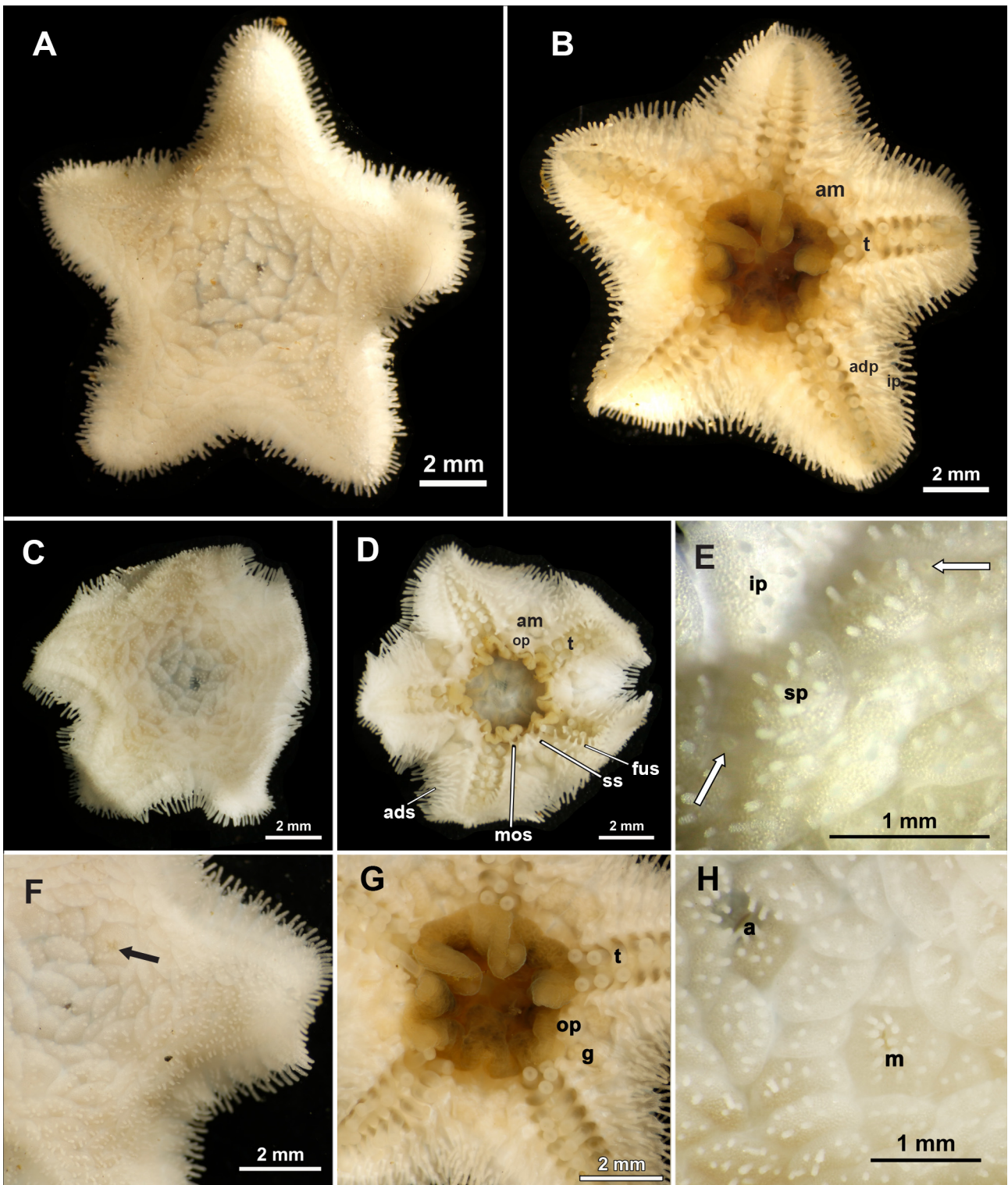
FIGURE 5. Light Microscopy images of *Caymanostella scrippscognaticausa* **sp. nov.** Paratype SIO-BIC E7289: A—live abactinal view; B—live actinal view; F—close-up live abactinal view, with arrow indicating madreporite; G—close-up live actinal view. Holotype SIO-BIC E11441: C—preserved abactinal view, with arrow indicating madreporite; D—preserved actinal view; E—abactinal interradius, with arrows indicating gonopores; H—abactinal central disc showing madreporite. Abbreviations: a, anus; adp, adambulacral plates; ads, adambulacral spines; am, actinal membrane; fus, furrow spine; g, gonads; ip, inferomarginal plate; m, madreporite; mos, marginal oral spines; op, oral plate; sp, superomarginal plate; ss, suboral spines; t, tube feet.
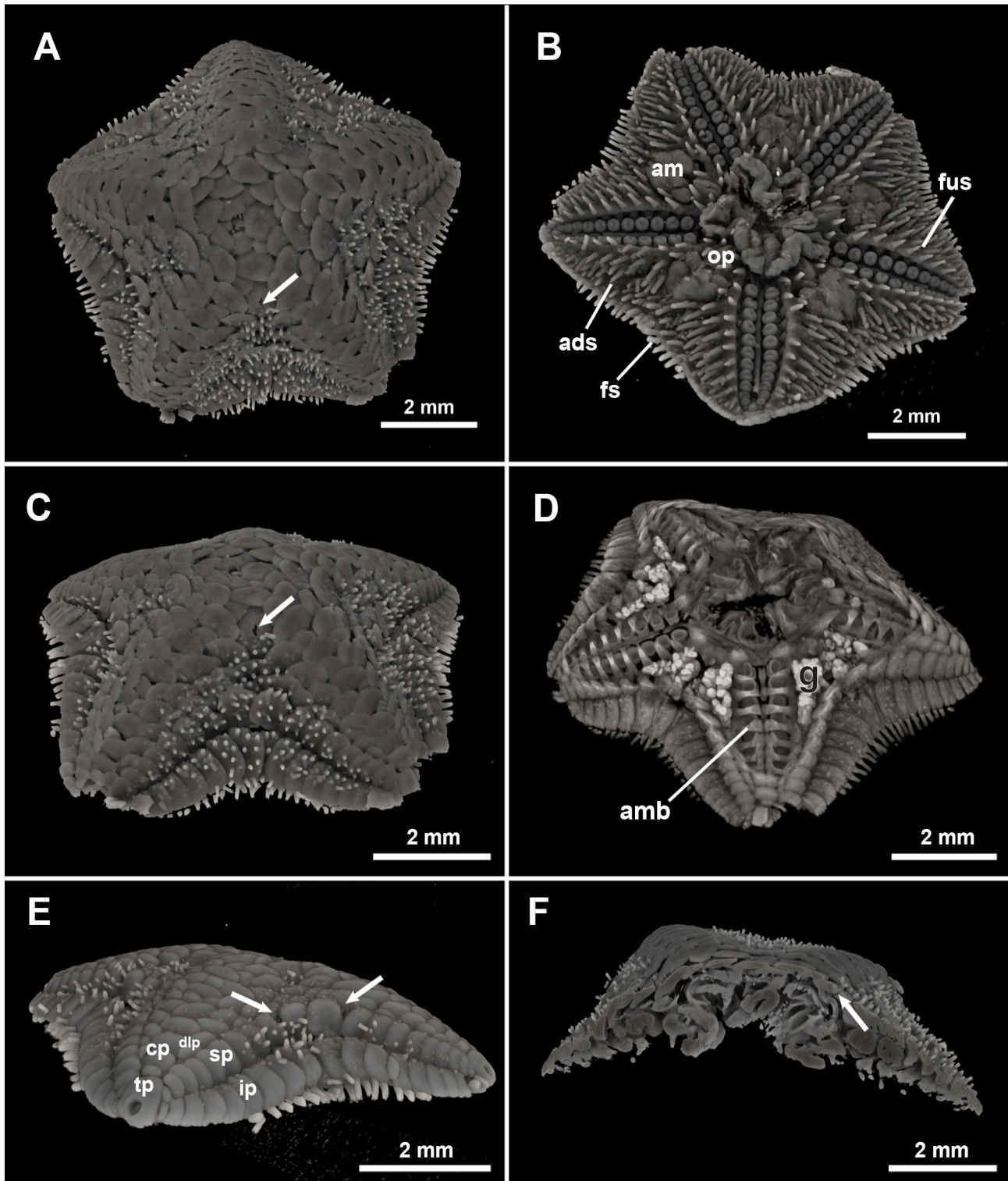
FIGURE 6. Compiled micro-CT scans of a paratype (SMF 6939) of *Caymanostella scrippscognaticausa* **sp. nov.** A, C—abactinal view, with arrow indicating madreporite; B—actinal view; D—abactinal internal view; E—lateral view of abactinal interradius with arrows indicating gonopores; F—abactinal view with cross section and arrow indicating madreporite and stone canal; R = 4.2 mm; r = 3.45mm. Abbreviations: ads, adambulacral spines; am, actinal membrane; amb, ambulacral plate; cp, carinal plate; dlp, distal-lateral plate; fs, fringe spines; fus, furrow spines; g, gonads; ip, inferomarginal plate; op, oral plate; ads, adambulacral spines; sp, superomarginal plate; tp, terminal plate.

proximal-most superomarginal plate, next to second proximal-most superomarginal plates (Figs 6E, 8B). Some gonopores appear slightly protruding, with narrow central slit, while others obscured by spines or epidermis and only visible with bleach treatment. Superomarginal plates and abactinal side of inferomarginal plates bear abactinal spines same as those on abactinal plates (superomarginal: 2–9 spinelets per plate, inferomarginal: 1–10 spinelets per plate) and similar density, but usually longer than those on central disc plates, especially those closer to margin (typical abactinal spines on superomarginal and inferomarginal plates = ~ 0.2 mm). On larger marginal plates, abactinal spines tend to arrange in two rows. Outer edge of each inferomarginal plate has 2 fringe spines. Fringe spines more elongated (0.44–0.49 mm) than abactinal spinelets and club-shaped, with tip wider than base, slightly compressed laterally (Fig. 8G, H). Lateral side of fringe spine wing-shaped (Fig. 8H), abactinal side with more thorns than actinal side.
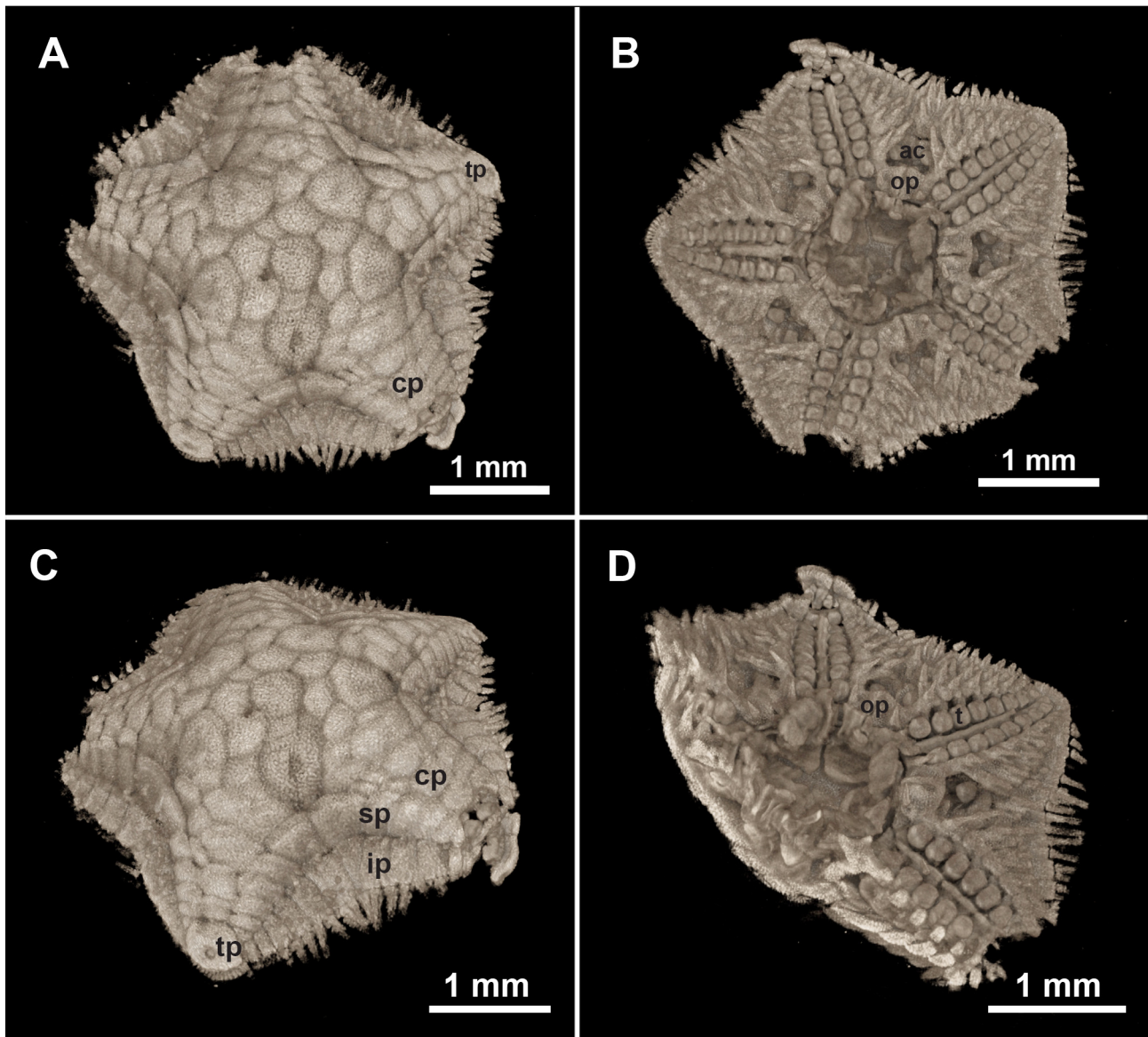
FIGURE 7. Compiled micro-CT scans of a sub-adult specimen (SMF 6938), identified as *Caymanostella scrippscognaticausa* **sp. nov.** A, C—abactinal view; B—abactinal view; D—actinal view with transection; R = 1.77 mm; r = 1.5 mm. Abbreviations: ac, actinal chamber; cp, carinal plate; tp, terminal plate; ip, inferomarginal plate; op, oral plate; sp, superomarginal plate; t, tube feet.
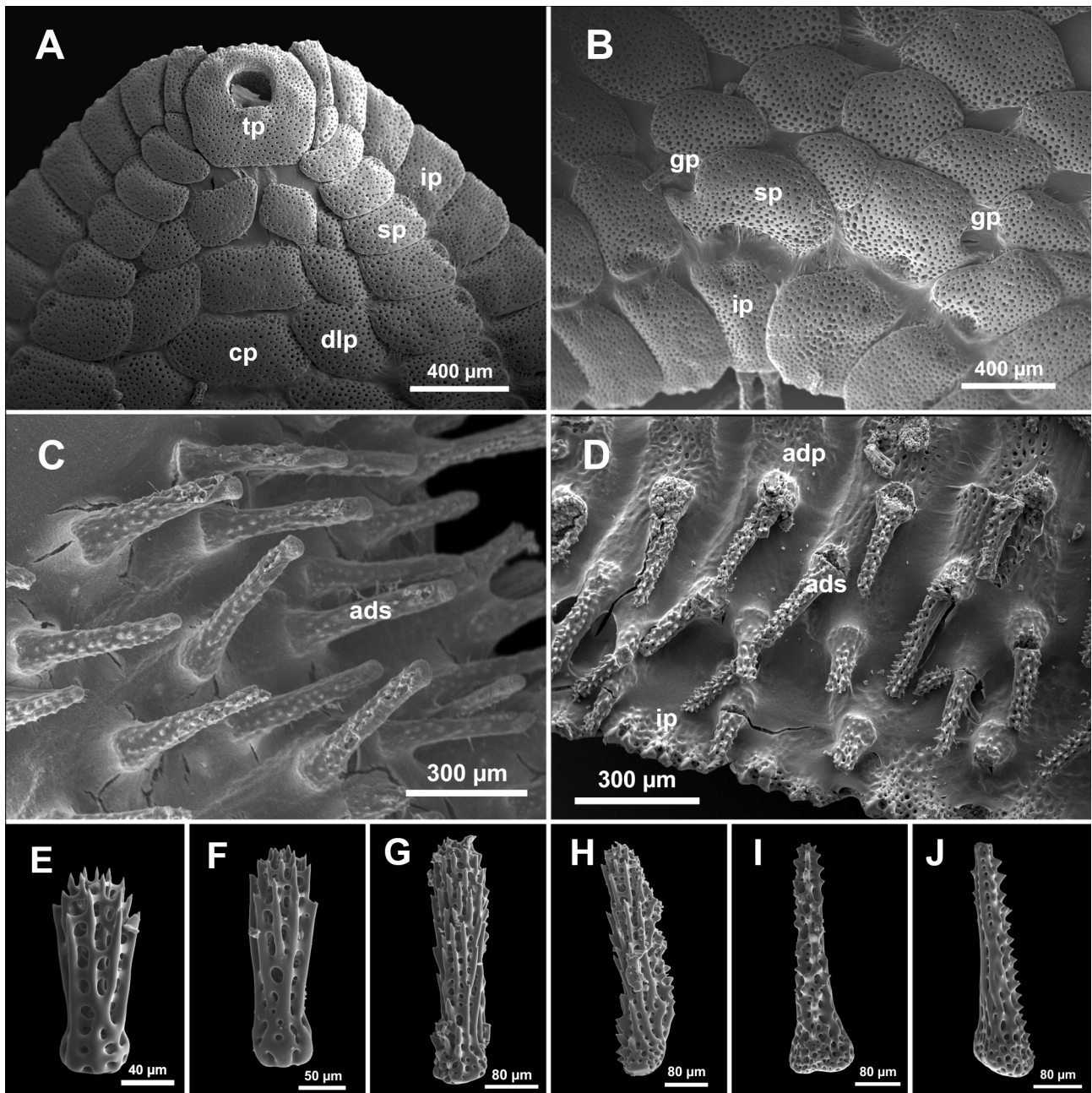
FIGURE 8. Scanning Electron Microscopy (SEM) images of *Caymanostella scrippscognaticausa* **sp. nov.** A—detail of bleached abactinal arm tip (paratype SIO-BIC E7290A); B—detail of bleached abactinal interradius (paratype SIO-BIC E7290A); C—detail of adambulacral spinelets on actinal side (paratype SIO-BIC E7290C); D—detail of bleached adambulacral spinelets on actinal side (paratype SIO-BIC E7290A); E, F—abactinal spinelets (paratype SIO-BIC E7290A); G—fringe spine, H—lateral view of fringe spine (paratype SIO-BIC E7290A); I—adambulacral spine, J—lateral view of adambulacral spine (paratype SIO-BIC E7290C); Abbreviations: adp, adambulacral plate; ads, adambulacral spine; cp, carinal plate; dlp, distal-lateral plate; gp, gonopore; ip, inferomarginal plate; sp, superomarginal plate; tp, terminal plate.

Ambulacral furrows narrow and slightly petaloid. Tube feet 12–14 pairs. Ambulacral plates elongate, with both ends wider than middle segment (Fig. 6D). 12 pairs of adambulacral plates between furrow and inferomarginals of each arm. Proximal-most plate square-shaped; distal-most plate square to triangular-shaped, both small. Rest bar-shaped, oriented perpendicularly to furrow and length decreases distally, with the second proximal-most adambulacral plate largest and most elongate. Adambulacral spines arrange in one or two alternating rows and pointing towards body margin similar angle as adambulacral plates (Fig. 8D). Number of adambulacral

spines on each plate vary with plate size. Proximal-most plate bears 1 adambulacral spine, while the number of adambulacral spines on the rest decreases distally with decrease in size, 5 at most. Adambulacral spines elongated (0.31–0.44 mm), thorny and robust (Fig 8D, I, J). Each tapers from wide base and numerous and small thorns tend to be obscured by the epidermis (Fig. 8C). The lateral side is smoother with few thorns. Each adambulacral plate has one furrow spine slightly pointing towards the ambulacral furrow. The oral side of inferomarginal plates also bears spines morphologically identical to adambulacral spines. The number of spines on the plate varies with plate size, with the largest, proximal-most plate bears 4 spines. Similar orientation as spines on adambulacral plates. Spines absent on plates near the arm tip. Oral opening large, around 2.85 mm wide. Stomach slightly everted. Paired oral plates at base of the interradius form a ridge in between. Each oral plate bears one suboral spine and 2 (sometimes 3) marginal spines pointing towards oral opening or furrow. Most pairs of oral plates at each interradius have the same number of spines, though sometimes one plate has 3 marginal spines while the other has 2. Spine shape and length are like adambulacral and furrow spines. Oral plates and proximal-most adambulacral plates delimit the boundary of the actinal chamber at the proximal part of the interradius, which contains two clusters of gonads separated by an inter-radial septum and covered by semi-transparent actinal membrane (Figs 5G, 6B).

TABLE 5. Variations of characters across ontogeny in *Caymanostella scrippscognaticausa* **sp. nov.**

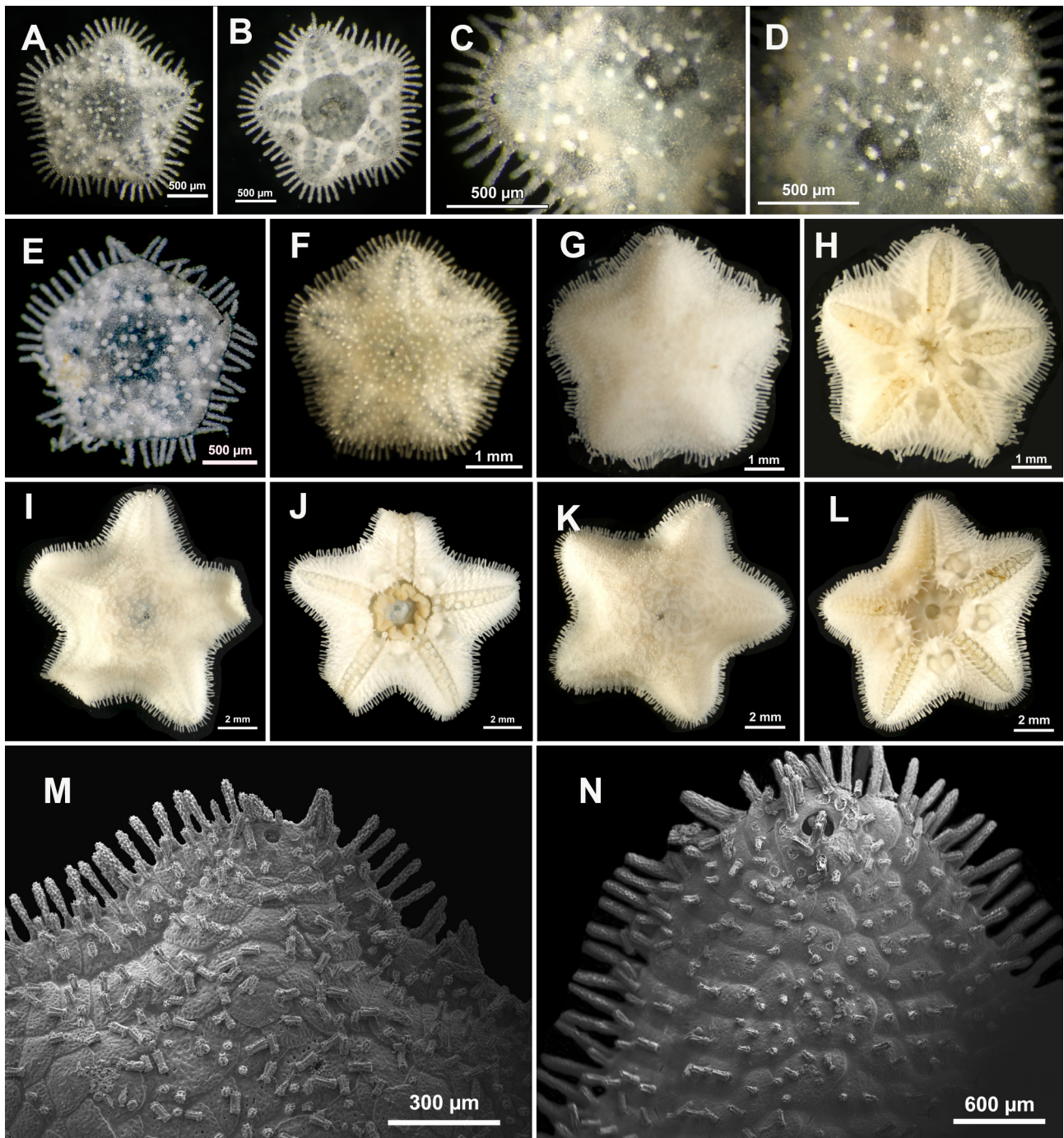| Morphological characters	Juvenile SIO-BIC E7228	Juvenile SIO-BIC E7075B	Subadult SIO-BIC SMF 6939	Large adult SIO-BIC E11441, holotype
R; r; R/r	R = 0.96 mm; r = 0.85 mm; R/r = 1.13	R = 1.85 mm; r = 1.53 mm; R/r = 1.21	R = 4.2 mm; r = 3.45 mm; R/r = 1.22	R = 5.85 mm, r = 4.15 mm, R/r = 1.41
Number of central disc plates	Central disc plates not discernable	9	~20	26
Central disc plate shapes and patterns	Not discernable	Irregularly oval with curved edges, with a single imbricating circle	Oval shaped or with curved edges, and imbricate in irregular circles	Irregularly oval with curved edges, and imbricate in irregular circles
Maximum number of abactinal spinelets on a central disc plate	Central disc plates not discernable	5	N/A, 7 in E11221A (R=2.88 mm)	12
Length of typical abactinal spinelets (mm)	~0.076	0.126	N/A, 0.136 in E11221A (R=2.88 mm)	0.150
Madreporite shape	Not visible	Single pore	Single slit	Branched grooves
Gonopore position	Not visible	Not visible	Visible, located at the gap between proximal edges of the first and second proximal-most superomarginal plates, notches not conspicuous	Visible, located in notches associated with the radial margin of the proximal-most superomarginal plates
Number of tube feet pairs per arm	5	7	12	12–14
Number of adambulacral plate pairs per arm	3	6	9	12

FIGURE 9. Light Microscopy (LM) and Scanning Electron Microscopy (SEM) images of *Caymanostella scrippscognaticausa* **sp. nov.** specimens across ontogeny. Juvenile, SIO-BIC E7228 (destroyed for DNA extraction) (R = 0.93 mm, r = 0.84 mm, R/r = 1.11): A—live abactinal view, B—live actinal view, C—close-up of preserved abactinal arm tip, D—close-up of preserved abactinal central disc. Juvenile, SIO-BIC E4403 (destroyed for DNA extraction) (R = 0.95 mm, r = 0.82 mm, R/r = 1.16): E—live abactinal view. Juvenile, paratype SIO-BIC E7075B (R = 1.85 mm, r = 1.53 mm, R/r = 1.21): F—live abactinal view, M—SEM abactinal arm. Sub-adult, paratype SIO-BIC E11221B (R = 3.04 mm, r = 2.35 mm, R/r = 1.30): G—preserved abactinal view; H—preserved actinal view. Adult, paratype SIO-BIC E7290C (R = 5.88 mm, r = 3.75 mm, R/r = 1.57): I—preserved abactinal view; J—preserved actinal view. Adult, paratype SIO-BIC E7290F (R = 5.99 mm, r = 4.11 mm, R/r = 1.46): K—preserved abactinal view; L—preserved actinal view. Adult, paratype SIO-BIC E7290C (R = 5.88 mm, r = 3.75 mm, R/r = 1.57): N—SEM abactinal arm tip.
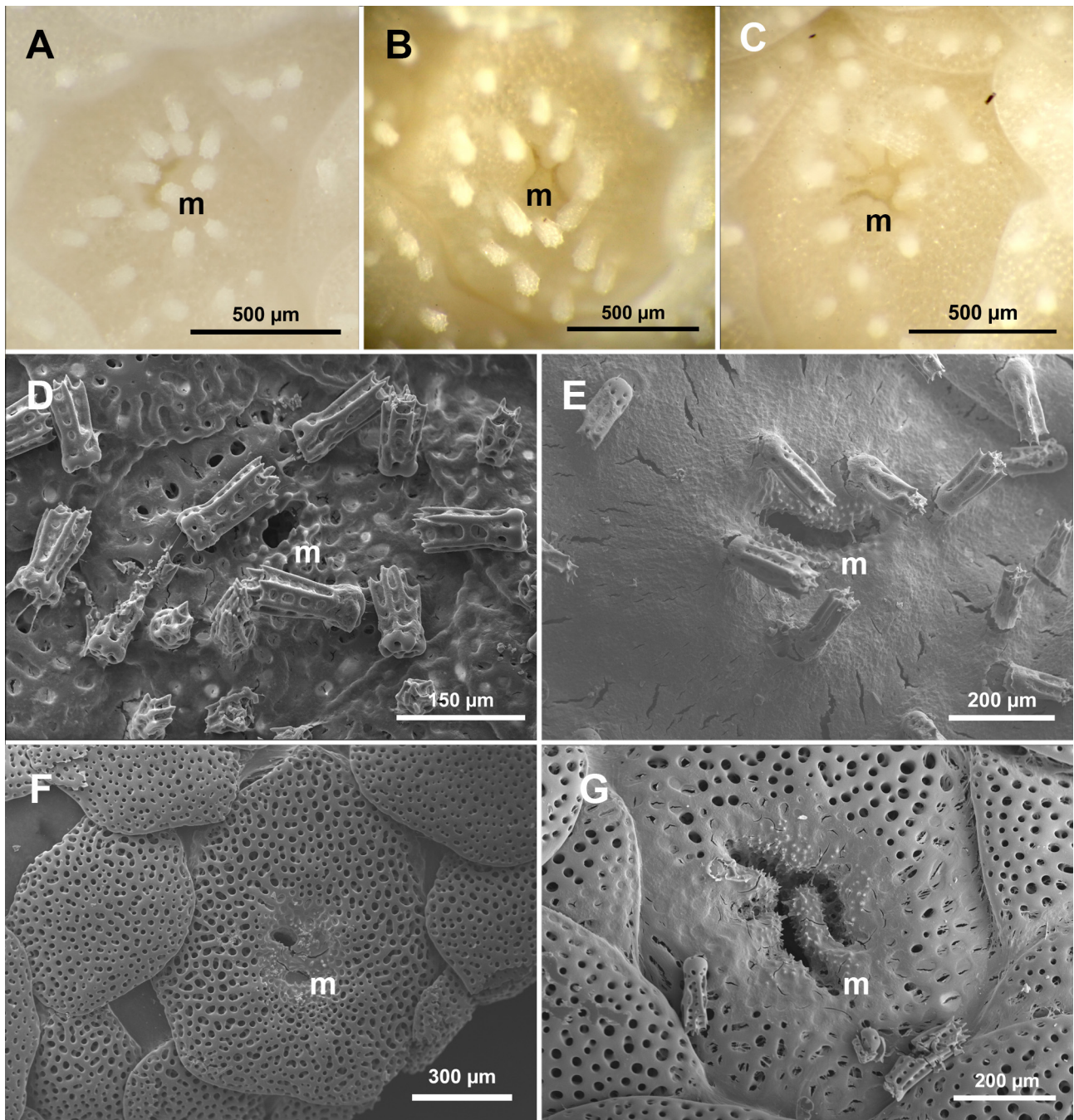
FIGURE 10. Light Microscopy (LM) and Scanning Electron Microscopy (SEM) images of madreporites among *Caymanostella scrippscognaticausa* **sp. nov.** specimens. A—holotype SIO-BIC E11441 (R = 5.85 mm, r = 4.15 mm, R/r = 1.41). B—paratype SIO-BIC E7290F (R = 5.99 mm, r = 4.11 mm, R/r = 1.46). C—paratype SIO-BIC E7289 (R = 6.85 mm, r = 4.65 mm, R/r=1.47). D—paratype SIO-BIC E7075B (R = 1.85 mm, r = 1.53 mm, R/r = 1.21). E—paratype SIO-BIC E7290C (R = 5.88 mm, r = 3.75 mm, R/r = 1.57). F—paratype SIO-BIC E7290A (R = 5.55 mm, r = 3.85 mm, R/r = 1.45). G—paratype SIO-BIC E7290D (R = 5.37 mm, r = 3.04 mm, R/r = 1.77, bent, measurement may not be accurate).

Variation. Specimens of *Caymanostella scrippscognaticausa* **sp. nov.** vary greatly in size (see description), likely representing different life stages. There were 7 clearly juvenile specimens among the collected specimens (R = 0.93–1.86 mm; r = 0.82–1.53 mm; R/r = 1.11–1.27), among which the smallest two were used up for DNA extraction (Table 1). Variations in several characters tend to correlate with ontogeny and body size. Smaller and less mature specimens are more pentagonal than stellate (adult average R/r = 1.40; juvenile average R/r = 1.20; Table 5), and early-stage juveniles are much thinner, almost transparent (Fig. 9A–F). Abactinal surfaces tend to be more

convex in large specimens. Both epidermis and abactinal plates appear thicker in large specimens. This results in a more uneven surface of the abactinal side (e.g., compare Fig. 9G and 9K). Under SEM the margin of the plates can be more obscured by the thicker epidermis (Fig. 9N) in comparison with juvenile specimens (Fig. 9M). Central disc plates arrange in more complex and less discernible cycles in large specimens due to greater number of plates, and orientation of plates and imbrication patterns can be more irregular (Table 5). The row of carinal plates is more discernible in small specimens (Fig. 7A, C). Small specimens have madreporites in a single slit or pore (single slit Fig. 6A, C; single pore Fig. 10D; Table 5), and although single pore/single groove madreporites have also been found in some large individuals (Fig. 10E, F), more complex madreporites with branching grooves are only present in large specimens (Fig. 10A–C, G; Table 5). Abactinal spinelets of the smallest juveniles (R = <1 mm) are less dense and significantly shorter (Table 5). While plates are not distinguishable in the smallest juveniles, terminal pores are visible at the abactinal side of each arm tip (Fig. 9A, C). The furrows are wide among the smallest juveniles and tube feet can be transparent in live specimens (Fig. 9B). Number of tube feet, disc plates, and adambulacral plates also increase with body size (Table 5). Some other non-ontogenetic variations can be observed: in some specimens the furrow spines point vertically rather than pointing towards the furrow; actinal chambers range from triangular to heart shaped. Paratype SIO-BIC E7290F showed all oral plates with 3 marginal oral spines.

Distribution. Known only from the Pacific margin of Costa Rica, confirmed from 990–1010 m and possibly with a broader depth range.

Remarks. The stellate body shape and spiniform abactinal armament of *Caymanostella scrippscognaticausa* **sp. nov.** are like that of *C. laguardai* (Table 6; Martin-Cao-Romero *et al.* 2021). However, the abactinal spinelet distribution of *C. scrippscognaticausa* **sp. nov.** appears sparser than that of *C. laguardai*, allowing the plates underneath to be exposed. Abactinal spinelets are similar in form to those of *Caymanostella spinimarginata* and *C.* cf. *spinimarginata* (Table 6; Dilman *et al.* 2022), but the tips appear not as wide as those in *C.* cf. *spinimarginata*. The position of the gonopore is the most like that of *C. spinimarginata* (Table 6; Dilman *et al.* 2022; Rowe 1989). Shapes and patterns of central disc plates are different from those in *C. admiranda* and *C. madagascarensis* (Table 6). Detailed morphological comparisons are listed in Table 6. The maximum uncorrected intraspecific COI distance of *C. scrippscognaticausa* **sp. nov.** was 1.8% (Table 3). There was a 6.4% divergence in uncorrected 16S between *C. scrippscognaticausa* **sp. nov.** and its well-supported sister taxon, *C. laguardai* (Fig. 3; Table 4).

Identification of the sub-adult SMF 6938 was uncertain since many characters can change with ontogeny. It is provisionally identified as *C. scrippscognaticausa* **sp. nov.** due to its overall similarity to the juvenile paratype E7075B (which was sequenced), and the somewhat square-shaped terminal plate, yet there are no *C. davidalani* **sp. nov.** specimens of a similar size or life stage to provide a definitive comparison.

Etymology. *Caymanostella scrippscognaticausa* **sp. nov.** is named after the Scripps Family group "Cousins for Causes" for their kind donation to support research in this study.

Caymanostella davidalani **sp. nov.**
Figures 11–13

Alvarado *et al.* (2022) Table 1, as *Belyaevostella* sp. *Caymanostella* sp.

Diagnosis. Body subpentagonal. Thin epidermis. Arms broad. Abactinal plates oval to polygonal shaped with curved margin, tightly overlapping. Abactinal armament spiniform and sparsely distributed. Central disc plates imbricate irregularly. One row of dorsal-lateral plates on each side of a row of carinal plates. Terminal plate rectangular-shaped. Each inferomarginal plate larger than the adjoining superomarginals. Gonopores visible, located in notches at the radial margin of the proximal-most superomarginal plates. Adambulacral spines thorny, narrow and elongated.

Materials Examined. Holotype: SIO-BIC E7101 (prepared for SEM), on wood at Seamount 2, Costa Rica, 8.8003°N, 85.1899°W, 1837 m depth, June 9, 2017, HOV *Alvin* dive 4926, collectors Greg Rouse and Josh Sisson [GenBank COI = PP627124; 16S = PP572463; H3= PP658047]. **Paratype:** MZUCR ECH2403, on wood at Mound 12, Costa Rica, 8.9325°N, 84.3074°W, 1002 m depth, June 5, 2017, HOV *Alvin* dive 4922, collectors Jen Le and Chris Roman. **Other materials:** SIO-BIC E7226 (specimen completely used up for DNA extraction; GenBank COI = PP627128), on deployed wood at Jaco Scar, Costa Rica, 9.1146°N, 84.8356°W, 1845 m depth, October 18, 2018, HOV *Alvin* dive 4972, collectors Greg Rouse and Avery Hiley; SIO-BIC E7238 (specimen completely used up for

DNA extraction; GenBank COI = PP627127), SIO-BIC E7242 (specimen completely used up for DNA extraction; GenBank COI = PP627126), on wood trap at Jaco Scar, Costa Rica, 9.1151°N, 84.8398°W, 1887 m depth, October 22, 2018, HOV *Alvin* dive 4976, collectors Shana Goffredi and Drew Bewley.
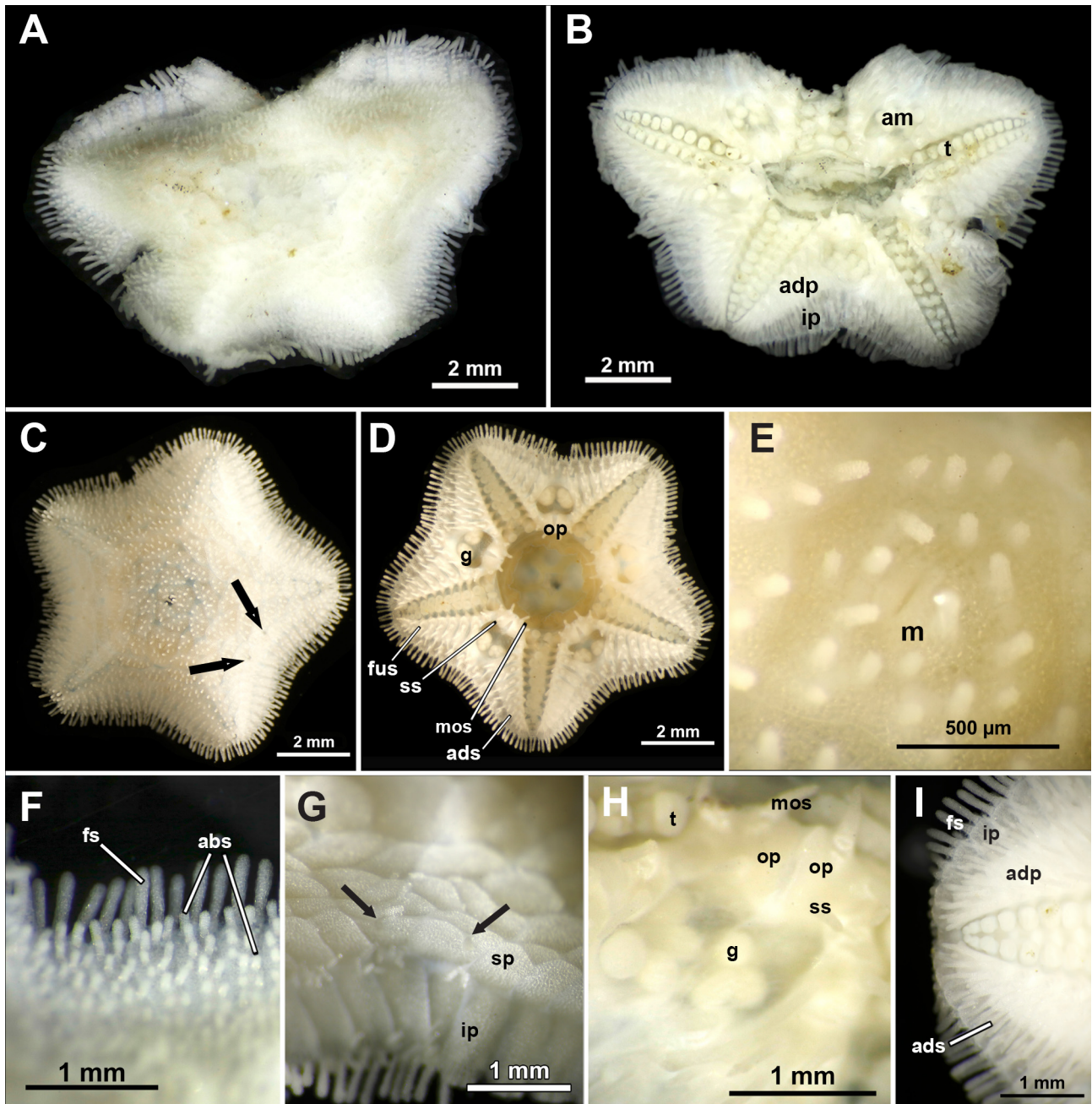

FIGURE 11. Light Microscopy (LM) images of *Caymanostella davidalani* **sp. nov.** Holotype SIO-BIC E7101, the missing arm was used for DNA extraction: A—preserved abactinal view; B—preserved actinal view; F—close-up of preserved abactinal arm margin; G—close-up of bleached abactinal interradius, with arrows indicating gonopores; H—close up of preserved interradial chamber containing gonads covered by actinal membrane; I—close up of preserved actinal arm tip. Paratype MZUCR ECH2403: C—live abactinal view, with arrows indicating gonopores; D—live actinal view; E—close-up of the madreporite. Abbreviations: abs, abactinal spinelets; adp, adambulacral plates; ads, adambulacral spines; am, actinal membrane; fs, fringe spines; fus, furrow spines; g, gonads; ip, inferomarginal plate; m, madreporite; mos, marginal oral spines; op, oral plate; sp, superomarginal plate; ss, suboral spines; t, tube feet.
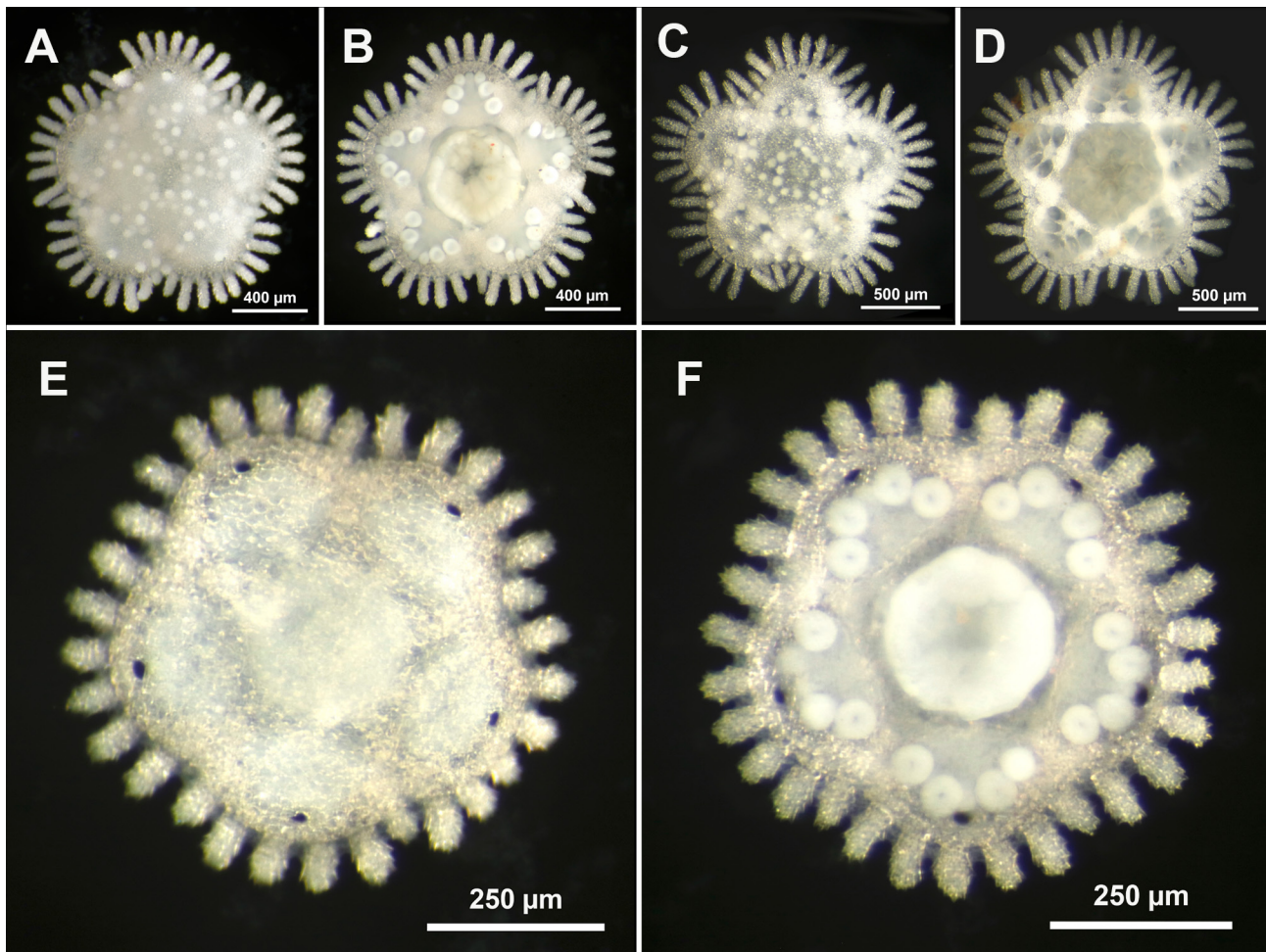
FIGURE 12. Light Microscopy (LM) images of *Caymanostella davidalani* **sp. nov.** juveniles. SIO-BIC E7226 (destroyed for DNA extraction): A—preserved abactinal view; B—preserved actinal view. SIO-BIC E7242 (specimen completely used up for DNA extraction): C—live abactinal view; D—live actinal view. SIO-BIC E7238 (destroyed for DNA extraction): E—preserved abactinal view; F—preserved actinal view.

Description. Adult body subpentagonal (Range of adult specimens: R = 4.30–5.19 mm, r = 3.34–4.15 mm, R/r = 1.25–1.28; Holotype R = 5.19 mm, r = 4.15 mm, R/r = 1.25, bent, measurement may not be accurate). Thin epidermis covers abactinal and actinal surface, dissolves easily with bleach. Abactinal plates irregularly oval-shaped with curved edges and imbricate distally. These plates overlap tightly, and outline of plates may be inconspicuous. Central disc plates oval to polygonal with curved edges, irregularly imbricating. Central disc plates covered with elongated and spiniform abactinal spinelets of various lengths (0.08–0.24 mm). Spinelets consist of a smooth and sometimes wide base, stem with longitudinal ridges, and slightly expanded thorny crown (Fig. 13E, F). Other abactinal plates bear abactinal spinelets of similar shape with density ~30/mm². Most spines on central disc plates lost. Arms broad. One row of distal-lateral plate on each side of a somewhat discernable row of carinal plates, imbricating with irregular patterns (Fig. 13A). Terminal plate rectangular with pore, marginal edge slightly narrower (Fig. 13A) and bearing abactinal spinelets slightly longer and larger than other abactinal spinelets on the arm (>0.16 mm). Two fringe spines (0.45 mm) at the margin of each terminal plate. Madreporite not visible on the holotype, but visible in paratype MZUCR ECH2403, appearing as a single slit (Fig. 11E).

One row of superomarginal plates and one row of inferomarginal plates are parallel with each other along each side of the arm. Both rows are imbricating. Inferomarginal plates are more elongated and rectangular, longer than wide. Superomarginals are of similar shape but smaller than inferomarginals. The proximal-most superomarginal plates differ from the other superomarginals in being much larger in size and almost oval-shaped, wider than long. The row of inferomarginals forms a flat and outstanding margin relative to the slightly convex abactinal surface

(Fig. 13A). Gonopores are present between the proximal edges of the first and second proximal-most superomarginal plates, each at a notch of the proximal-most superomarginal plate (Figs 11G, 13B). There are 13 or fewer abactinal spines per inferomarginal, similar in length to those on central disc plates (~0.13 mm) and those closer to the margin tend to appear longer (Fig. 11F). Distal-most abactinal spinelets on the inferomarginals are longer than other abactinal spinelets on the plate (>0.17 mm). There are 2–3 club-shaped fringe spines (0.45–0.52 mm) at the margin. Fringe spines are slightly compressed laterally, have more thorns on the abactinal side, and appear wing-shaped in lateral view (Fig. 13G, H).
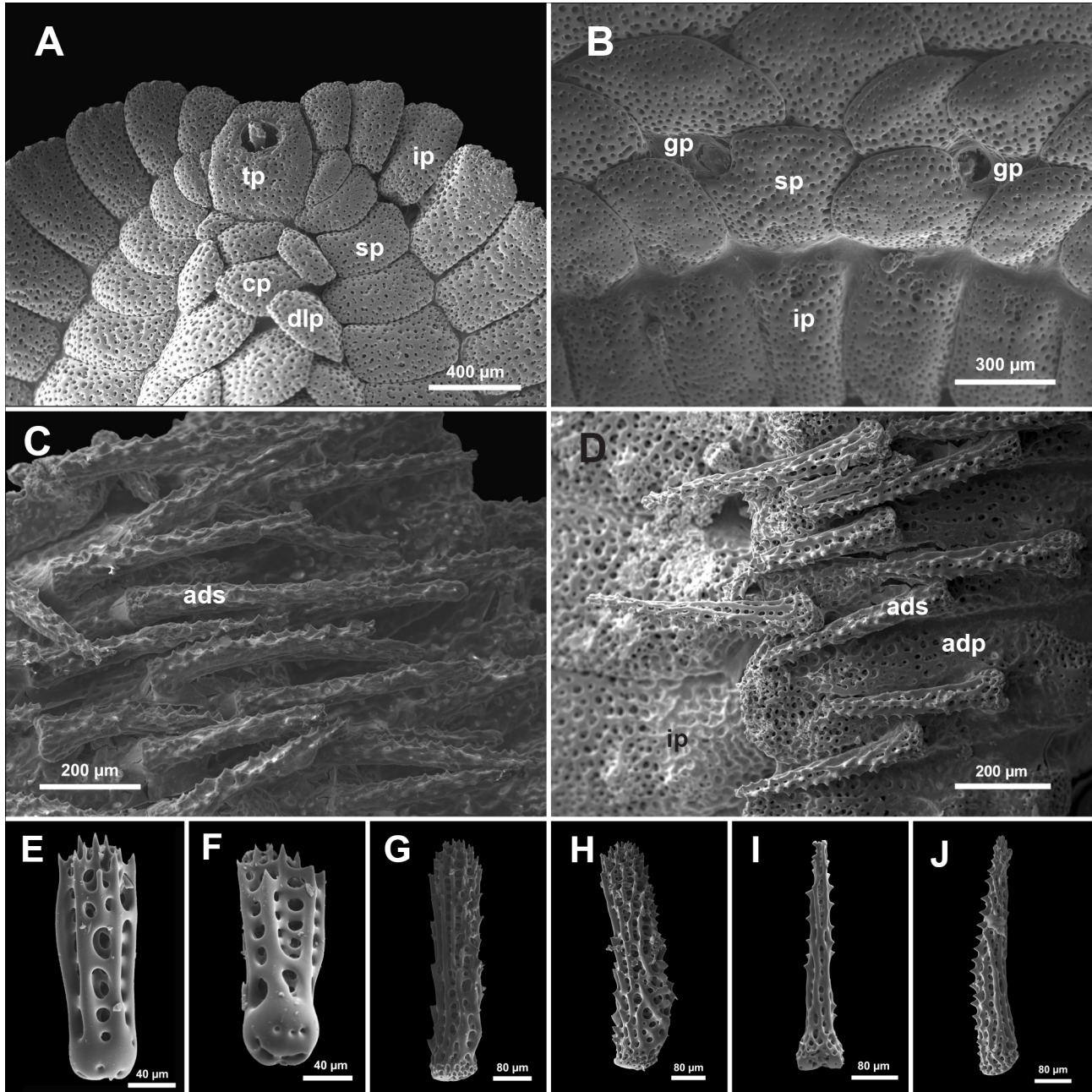

FIGURE 13. Scanning Electron Microscopy (SEM) images of *Caymanostella davidalani* **sp. nov.** A—detail of bleached abactinal arm tip (holotype SIO-BIC E7101); B—detail of bleached abactinal interradius (paratype MZUCR ECH2403); C—detail of adambulacral spinelets on actinal side (holotype SIO-BIC E7101); D—detail of bleached adambulacral spinelets on actinal side (holotype SIO-BIC E7101); E, F—abactinal spinelets (holotype SIO-BIC E7101); G—fringe spine, H—lateral view of fringe spine (holotype SIO-BIC E7101); I—adambulacral spine, J—lateral view of adambulacral spine (holotype SIO-BIC E7101); Abbreviations: adp, adambulacral plate; ads, adambulacral spines; cp, carinal plate; dlp, distal-lateral plate; gp, gonopore; ip, inferomarginal plate; sp, superomarginal plate; tp, terminal plate.

Ambulacral furrows slightly petaloid and each includes 12 pairs of tube feet. Bar-shaped adambulacral plates (10 pairs) bear adambulacral spines (0.39–0.67 mm) arranging in one or two alternating rows with uniform orientation towards body margin (Figs 11I, 13D), with larger plates having more spines. Each adambulacral plate has one furrow spine with varying orientations, from pointing towards the furrow to towards body margin like adambulacral spines. Adambulacral spines and furrow spines are tapering, thorny, and elongated (Figs 11I, 13C, D, I, J). There are few thorns on the lateral side. Adambulacral spines tightly lie on the adambulacral plates, pointing towards the body margin while obscuring the outline of the plates. The oral side of inferomarginal plates bears spines morphologically identical to adambulacral spines and with similar orientation. Oral opening is distorted, large, and with slightly everting stomach (Fig. 11B). Paired oral plates are at the base of the interradius and form a ridge in-between. Each oral plate has one suboral spine and two marginal spines pointing towards the oral opening, similar to adambulacral spines but wider (Fig. 11H). Actinal chambers are distorted, irregular in shape and contain gonads (Fig. 11H). Actinal chambers are located at the proximal part of the interradius and are bounded by the oral plates and the proximal-most adambulacral plates.

Variation. The limited material of *C. davidalani* **sp. nov.** does not allow for a detailed analysis of morphological variations across individuals and ontogeny. Paratype MZUCR ECH2403 (R = 4.3 mm, r = 3.34 mm, R/r = 1.28) is smaller, yet has a more conspicuous single-slit madreporite (Fig. 11E) and gonopores (Fig. 11C) than the holotype. Gonopores are present between proximal edges of the first and second proximal-most superomarginal plates, and are slightly protruding, with a narrow slit at the center. The abactinal spinelets are sparse, and inferomarginal plates do not form a flat and outstanding margin, but instead form a convex abactinal surface with the other plates. Differences in size and shape between inferomarginals and superomarginals are less conspicuous in MZUCR ECH2403. Gonad clusters are less developed, which indicates an early life stage compared to the holotype (Fig. 11D). Three early-stage juveniles (R = 0.31–0.68 mm; r = 0.28–0.55 mm; R/r = 1.10–1.24) (identities all confirmed by DNA) are more pentagonal than stellate (average R/r = 1.18) (Fig. 12A–F). The body of the juveniles is thin and semi-transparent. Abactinal armaments are few and short. Pores are visible at the arm tip (Fig. 12A, C–F). Ambulacral furrows are wide and tube feet can be transparent in live specimens (Fig. 13D). Tube feet of the smallest specimen (SIO-BIC E7238, Fig. 12E, F) form almost a circle outlining the body margin. All juveniles were used up for DNA extraction.

Distribution. Known only from the Pacific margin of Costa Rica, 1002–1887 m.

Remarks. The body shape of the *Caymanostella davidalani* **sp. nov.** holotype is not as stellate as in *C. scrippscognaticausa* **sp. nov.** of similar radii, yet more stellate than those of other species of *Caymanostella*. The epidermis appears thinner than that in *C. scrippscognaticausa* **sp. nov.** and more easily dissolved with bleach. Abactinal plates are thinner and overlap more tightly than those of *C. scrippscognaticausa* **sp. nov.**, so that the surface appears more even. Terminal plates tend to be more elongated (Fig.13A) than the square-shaped terminal plates of *C. scrippscognaticausa* **sp. nov.** (Fig. 8A). Comparing fully mature specimens, the arm tip of *C. davidalani* **sp. nov.** appears wider than that of *C. scrippscognaticausa* **sp. nov.** Because of the thin epidermis, thorns of adambulacral spines are more conspicuous in *C. davidalani* **sp. nov.** (Fig. 13C) than those in *C. scrippscognaticausa* **sp. nov.** (Fig. 8C). Adambulacral spines are generally longer and narrower in *C. davidalani* **sp. nov.** compared to those in *C. scrippscognaticausa* **sp. nov.** (Table 6). Juveniles and small paratypes of *C. scrippscognaticausa* **sp. nov.** (SMF 6939, Fig. 6; SIO-BIC E11221B, Fig. 9G, H) and *C. davidalani* **sp. nov.** (MZUCR ECH2403, Fig. 11C, D) are morphologically similar. The spiniform abactinal armament is like that of *C. laguardai* but less dense. The abactinal spinelets are like those of *C. scrippscognaticausa* **sp. nov.** (Table 6). The shape and pattern of the central disc plates are different from those in *C. admiranda* and *C. madagascarensis* (Table 6). The position of the gonopores is like those of *C. scrippscognaticausa* **sp. nov.** and *C. spinimarginata* (Table 6). Inferomarginals of *C. davidalani* **sp. nov.** are not as elongated as those of *Belyaevostella* (Rowe 1989; Fujita *et al.* 1994). Maximum uncorrected intraspecific COI distance of *C. davidalani* was 1.0% (Table 3). *C. davidalani* **sp. nov.** was recovered as sister to the clade of *C. scrippscognaticausa* **sp. nov.** and *C. laguardai* **sp. nov.**, and the three species formed a well-supported clade sister to *C.* cf. *spinimarginata* (Fig. 3). The minimum uncorrected divergence between *C. davidalani* **sp. nov.** and *C. scrippscognaticausa* **sp. nov.** was 10.5%, while the uncorrected 16S distance between *C. laguardai* and *C. davidalani* **sp. nov.** was 8.6% (Tables 3, 4).

A sub-adult paratype of *C. davidalani* **sp. nov.** (MZUCR ECH2403) was collected from the same piece of wood harboring several paratypes of *C. scrippscognaticausa* **sp. nov.** (Dive 4922, Mound 12, June 5, 2017, Fig. 2B), showing sympatry of the two species. Two juveniles (SIO-BIC E7238, E7242) were on the same wood trap (Dive 4976,

TABLE 6. Comparison of morphological characters of selected species in Caymanostellidae. Descriptions of new species (except R, r and R/r) are based on shared characters among adult specimens. Crinitostella is synonymized here as Caymanostella. *Not discernable according to Dilman et al. (2022), but visible in Fig. 2E of Dilman et al. (2022) and Rowe (1989).

Morphological characters	Caymanostella spinimarginata Belyaev, 1974	Caymanostella admiranda Belyaev & Litvinova, 1977	Caymanostella phorcynis Rowe, 1989	Caymanostella madagascarensis Belyaev & Litvinova, 1991	Caymanostella cf. spinimarginata (see Dilman et al. 2022)	Caymanostella scrippscognaticausa sp. nov.	Caymanostella davidalani sp. nov.	Caymanostella loresae sp. nov.	Caymanostella laguardai (Martin-Cao-Romer et al. 2021) n. comb.	Belyaevostella hispida (Aziz & Jangoux 1984)	Belyaevostella hyugaensis Fujita, Stampanato & Jangoux, 1994
R (mm); r (mm)	2–5; 1.75–4.50	3.35–4.90; 2.9–4.3	2.8–10.5; 2.2–8.5	2.0; 2.2	5.3–9.5; 4.5–6.5	0.93–6.85; 0.82–4.65	0.31–5.19; 0.28–4.15	5.36–6.72; 4.48–5.94	2.7–3.9; 1.1–2.9	5.3–13.6; interradius range unknown	10; 8
R/r	1.12–1.38	1.16–1.2	1.05–1.3	1.1	1.6–2.1 max R / min r	1.21–1.77	1.25–1.28	1.09–1.24	1.33–1.59	1.17	1.2
Central disc plate shapes and patterns (excluding primary interradials)	Imbricating in circles, uniformly fan shaped and similar in size	Irregularly imbricating, hex-heptagonal shaped, varying in size	Imbricating in circles, uniformly fan shaped and similar in size	Irregularly imbricating, polygonal shaped, varying in size	Imbricating in circles, uniformly fan shaped and similar in size	Imbricating in circles, irregularly oval to polygonal shaped with curved edges, mostly similar in size; imbrication patterns more irregular in large adults	Imbricating in circles, irregularly oval to polygonal shaped with curved edges, mostly similar in size	Imbricating irregularly, plates typically circular or subcircular and are similar in size	Imbricating in somewhat irregular circles, pentagonal to hexagonal shaped with curved edges	Irregularly imbricating, perforated and scale-like	Irregularly imbricating, subcircular
Madreporite shape	Slit-like opening	Single pore piercing small knobble	Not described	Slit-like opening	Multiple branching grooves	Single slit/pore to multiple branching grooves	Not visible in holotype; single slit in small paratype	Not visible in holotype; multiple branching grooves	Y-shaped	Not described	Inconspicuous
Row of carinal plates	Somewhat discernable *	Discernable	Discernable	Discernable	Not discernable	Discernable	Discernable	Discernable	Discernable	Not described	Discernable
Rows of dorsal-lateral plates on each side of carinal row	At least 2 rows (Rowe, 1989)	2–3 rows	3–6 rows	Not described	Not described	1 row, sometimes 2 rows towards proximal end	1 row	1 row, absent near arm tip	1 row	Not described	Not discernable
Inferomarginal and adjoining superomarginal plate size	Similar in size	Similar in size	Similar in size	Similar in size	Inferomarginal slightly larger than superomarginal plate	Inferomarginal slightly more elongated than superomarginal plate	Inferomarginal more elongated than superomarginal plate	Inferomarginals elongated than superomarginals	Similar in size	Superomarginals square in juveniles, elongated in adults but smaller than elongated inferomarginals	Inferomarginals more elongated than superomarginals

TABLE 6. (Continued)

Morphological characters	Caymanostella spinimarginata Belyaev, 1974	Caymanostella admiranda Belyaev & Litvinova, 1977	Caymanostella phorcynis Rowe, 1989	Caymanostella madagascarensis Belyaev & Litvinova, 1991	Caymanostella cf. spinimarginata (see Dilman et al. 2022)	Caymanostella scrippscognaticausa sp. nov.	Caymanostella davidalani sp. nov.	Caymanostella loresae sp. nov.	Caymanostella laguardai (Martin-Cao-Romer et al. 2021) n. comb.	Belyaevostella hispida (Aziz & Jangoux 1984)	Belyaevostella hyugaensis Fujita, Stampanato & Jangoux, 1994
Gonopores position	In notches on the proximal marginal of two proximal-most superomarginal plates	Piercing the two proximal-most superomarginal plates	Piercing the two proximal-most superomarginal plates	Not visible	In notches on the proximal marginal of two proximal-most superomarginal plates	In notches on the proximal margin of two proximal-most superomarginal plates	In notches on the proximal margin of two proximal-most superomarginal plates	Piercing the two proximal-most superomarginal plates	No conspicuous gonopores	Between the two diverging, proximal-most superomarginals	Between the two diverging, proximal-most superomarginals; proximal ends of the two proximal-most inferomarginals also diverge due to uncalcified area
Abactinal armaments	Spiniform, wide base and expanded crown	Granuliform, wider than long; dome-shaped with narrow and sharp thorns (Dilman et al., 2022)	Granuliform, dome-shaped	Granuliform, rounded	Spiniform, wide base and expanded crown	Spiniform, wide base, longitudinal ridges and slightly expanded crown	Spiniform, wide base, longitudinal ridges and slightly expanded crown	Granuliform, longer than wide; crown dome-shaped with small thorns; base short and smooth	Spiniform, with longitudinal ridges and slightly expanded crown	Spiniform and elongated	Spiniform, slightly sacculated at base
Fringe spines	Elongated; abactinal/actinal view club-shaped; slightly compressed laterally; lateral view wing-shaped; longitudinal ridges somewhat discernable	Elongated; abactinal/actinal view club-shaped; slightly compressed laterally; lateral view wing-shaped; dense small thorns; no longitudinal ridges (Dilman et al., 2022)	Elongated; abactinal/actinal view club-shaped	Elongated; flattened abactinal-actinal direction; bear longitudinal ridges (Dilman et al., 2022)	Elongated; abactinal/actinal view club-shaped; slightly compressed laterally; lateral view wing-shaped; longitudinal ridges somewhat discernable	Elongated; abactinal/actinal view club-shaped; slightly compressed laterally; lateral view wing-shaped; bear longitudinal ridges	Elongated; abactinal/actinal view club-shaped; slightly compressed laterally; lateral view wing-shaped; bear longitudinal ridges	Elongated; abactinal/actinal view club-shaped; slightly compressed laterally; lateral view wing-shaped; dense small thorns; no longitudinal ridges	Elongated; abactinal/actinal view club-shaped; bear longitudinal ridges	Elongated	Elongated and stout

TABLE 6. (Continued)

Morphological characters	*Caymanostella spinimarginata* Belyaev, 1974	*Caymanostella admiranda* Belyaev & Litvinova, 1977	*Caymanostella phorcynis* Rowe, 1989	*Caymanostella madagascarensis* Belyaev & Litvinova, 1991	*Caymanostella* cf. *spinimarginata* (see Dilman *et al.* 2022)	*Caymanostella scrippscognaticausa* sp. nov.	*Caymanostella davidalani* sp. nov.	*Caymanostella loresae* sp. nov.	*Caymanostella laguardai* (Martin-Cao-Romer *et al.* 2021) n. comb.	*Belyaevostella hispida* (Aziz & Jangoux 1984)	*Belyaevostella hyugaensis* Fujita, Stampanato & Jangoux, 1994
Abactinal papulae	Absent	Absent	Absent	Absent	Absent	Absent	Absent	Absent	Absent	Present	Present
Spicules in actinal membrane	Absent	Absent	Absent	Absent	Absent	Absent	Absent	Absent	Absent	Present, perforated plate-like	Present, perforated plate-like
Distribution	Cayman Trench, 6740–6780 m; 2475–6790 m (Dilman *et al.*, 2022)	Coral Sea, Timor Sea and Celebes Seas, 520–5220 m (Dilman *et al.*, 2022)	Tasman Sea, South Pacific Ocean, 736–1208 m; Celebes Sea, 2053 m (uncertain record Rowe, 1989)	Off west coast of Madagascar, 1500 m	Kuril-Kamchatka Trench, 5101–5134 m	Pacific margin of Costa Rica, 990–1010 m	Pacific margin of Costa Rica, 1002–1887 m	Tamayo Fracture Zone, Gulf of California, 3054 m	Off Tabasco, Gulf of Mexico, 418–427 m	East Indian region off North-East coast of Australia, 1301–2350 m	Hyuga Basin, off southern Japan, 1650–1653 m

deployed May 29, 2017, and recovered October 22, 2018) where the holotype of the ribbon worm *Alvinonemertes christianeae* Sagorny, von Döhren, Rouse & Tilic, 2022 was collected (Sagorny *et al.* 2022).

Etymology. *Caymanostella davidalani* **sp. nov.** is named for David Alan Lewis, in appreciation of his support of marine biodiversity research and the Scripps Institution of Oceanography Benthic Invertebrate Collection.

Caymanostella loresae sp. nov.
Figures 14–16

Diagnosis. Body pentagonal or subpentagonal. Thick epidermis. Dense and granuliform abactinal armaments. Central disc plates circular, imbricating irregularly. Gonopores visible, piercing through the proximal-most superomarginal plates. Madreporite with branching grooves. One row of dorsal-lateral plates on each side of a row of carinal plates until arm tip. Terminal plate slightly trapezoidal. Inferomarginals more elongate than adjoining superomarginals. Short adambulacral spines covered with thick epidermis.

Materials examined. Holotype: ICML-EMU-13880 (formerly SIO-BIC E11477), on wood at Tamayo Fracture Zone, Gulf of California, Mexico, 22.9628°N, 108.1576°W, 3054 m depth, April 11, 2003, ROV *Tiburon* dive 553, collector Bob Vrijenhoek and party. **Paratypes:** SMF 6940 (prepared for μCT), E11393B (prepared for SEM), SIO-BIC E11393C, SIO-BIC E11393D, USNM 1487403 [GenBank COI= PP627129; 16S=PP572464; H3= PP658051], same collection data as holotype; USNM 1487403 was ethanol-fixed and the other five specimens were formalin-fixed.

Description. Adult body pentagonal to subpentagonal (R = 5.36–6.72 mm, r = 4.48–5.94 mm, R/r = 1.09–1.24; Holotype R = 6.47 mm, r = 5.86 mm, R/r =1.10, bent, measurement may not be accurate). Thick epidermis and dense armaments obscure plates. Abactinal side, excluding the inferomarginal plates, is slightly convex. Central disc plates differ from other abactinal plates in their mainly circular to subcircular shapes, imbricating irregularly. Other abactinal plates show regular distally imbricating patterns. Five primary inter-radial plates are irregular in shape and large. Madreporite has multiple branching grooves and is obscured by abactinal granules and epidermis (Figs 14E, 15B). Arms are wide, with oval to pentagonal abactinal plates more elongated relative to central disc plates. One row of distal-lateral plates on each side of the carinal plates that can be absent near arm tip (Fig. 16A). Terminal plate slightly trapezoidal, with distal end wider than proximal end (Fig. 16A).

Parallel rows of pentagonal superomarginal plates and inferomarginal plates along the body margin, imbricating radially, 9–10 plates each. Each inferomarginal plate is more elongated than the adjoining superomarginal plate (Figs 15B, C, 16A). The proximal-most superomarginal plates are oval-shaped and the largest, wider than long. One gonopore pierces through each of the proximal-most superomarginal plates (Figs 14A, C, E, 15B, 16B). All abactinal plates and abactinal side of marginal plates covered and obscured by dense small and round abactinal granules (0.06–0.1 mm, density>80/mm^2). Abactinal granules consist of a smooth short base and a spikey dome-shaped crown (Fig. 16E, F). Granules tend to be larger, more elongated and more cone-shaped around gonopores, terminal pores and near the distal edge of inferomarginal plates. Fringe spines (0.37–0.47 mm) club shaped from actinal/abactinal views and wing-shaped from lateral views. With many small pores and thorns, which are denser on the abactinal side (Fig. 16G, H). No obvious longitudinal ridges along the spines. Two fringe spines attach to the margin of each inferomarginal plate. There are 2–3 fringe spines at the margin of each terminal plate.

Ambulacral furrows slightly petaloid and each has 11–14 pairs of tube feet. Bar-shaped adambulacral plates (10–11 pairs in bleached paratype, Fig. 14D, F) obscured by adambulacral spines and epidermis. Adambulacral spines (0.4–0.69 mm) are tapering with wide base and are covered by thick epidermis (Fig. 16C, D, I, J). They orient towards the body margin, aligned with the adambulacral plates (Fig. 16C). Each adambulacral plate bears one furrow spine similar to adambulacral spines, but orient either perpendicular to the plates or pointing towards the furrow (Figs 14F, 15A). The oral side of inferomarginal plates have spines morphologically identical to adambulacral spines, also orienting towards body margin. Thick epidermis and dense spines obscure plate outlines. Paired oral plates are at the base of the interradius and form a ridge in-between. Each oral plate bears two suboral spines and 3 (sometimes 2) marginal oral spines pointing towards the interradius (Fig. 14B, F). In some cases, the number marginal oral spines on the paired oral plates differ, with one bearing 3 while the other bearing 2. Oral opening round and wide (~4 mm), and the stomach slightly everted in the holotype. Actinal chambers triangular to heart-shaped, each containing two clusters of gonads separated by an interradial septum (Fig. 14B, D, F).
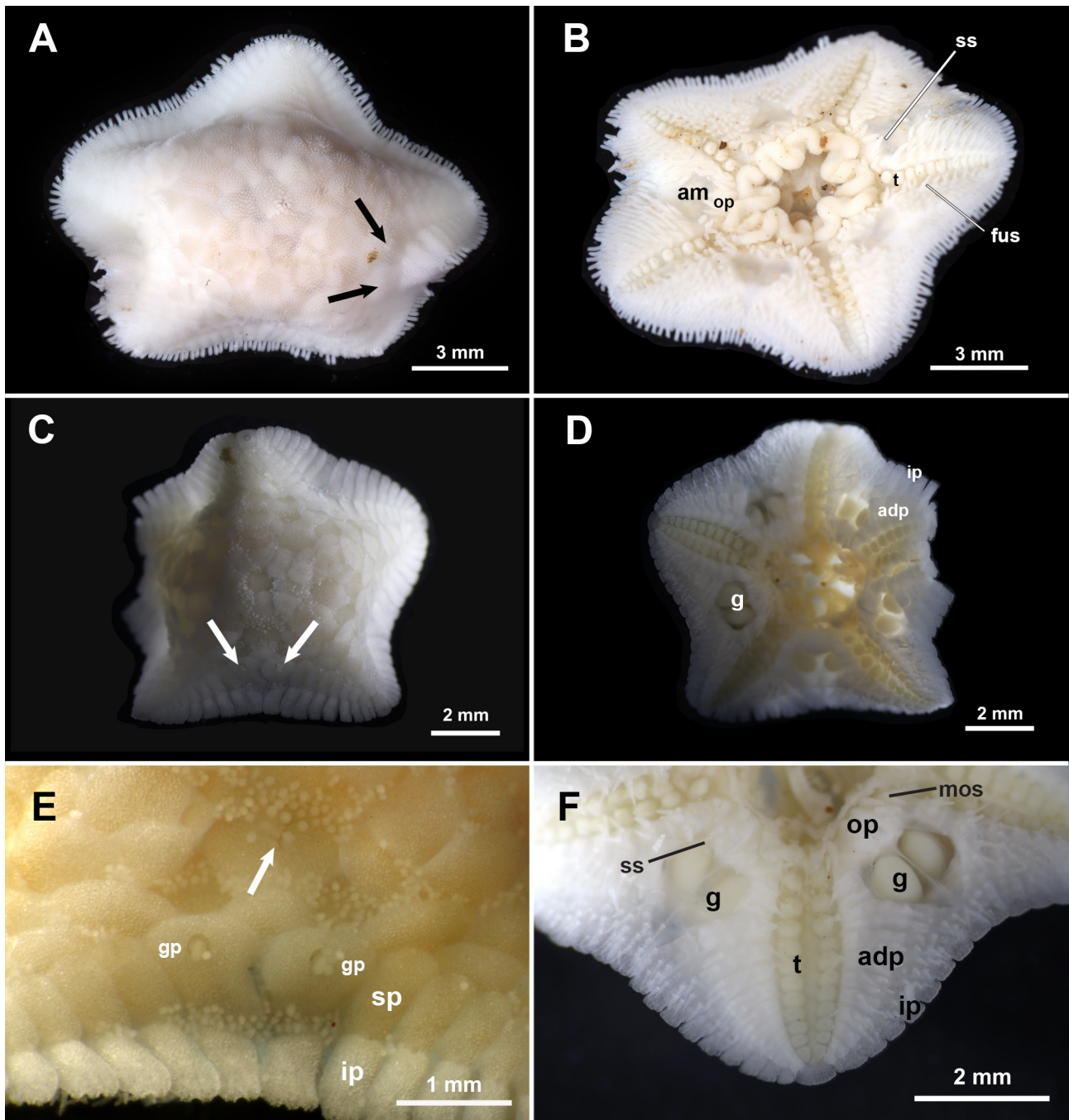
FIGURE 14. Light Microscopy (LM) images of *Caymanostella loresae* **sp. nov.** Holotype ICML-EMU-13880: A—preserved abactinal view, with arrows indicating gonopores; B—preserved actinal view. Paratype SIO-BIC E11383B: C—bleached abactinal view, with arrows indicating gonopores; D—bleached actinal view; E—close-up of bleached abactinal interradius, with arrow indicating madreporite; F—close-up of bleached actinal arm. Abbreviations: adp, adambulacral plates; am, actinal membrane; fus, furrow spines; g, gonads; gp, gonopore; ip, inferomarginal plate; mos, marginal oral spines; op, oral plate; sp, superomarginal plate; ss, suboral spines; t, tube feet.

Variation. All paratypes are fully mature and are morphologically similar. Gonopores and madreporites obscured by dense abactinal granules and only become visible after removing tissues and granules with bleach.

Distribution. Known only from Tamayo Fracture Zone, Gulf of California (Mexico), at 3054 m.
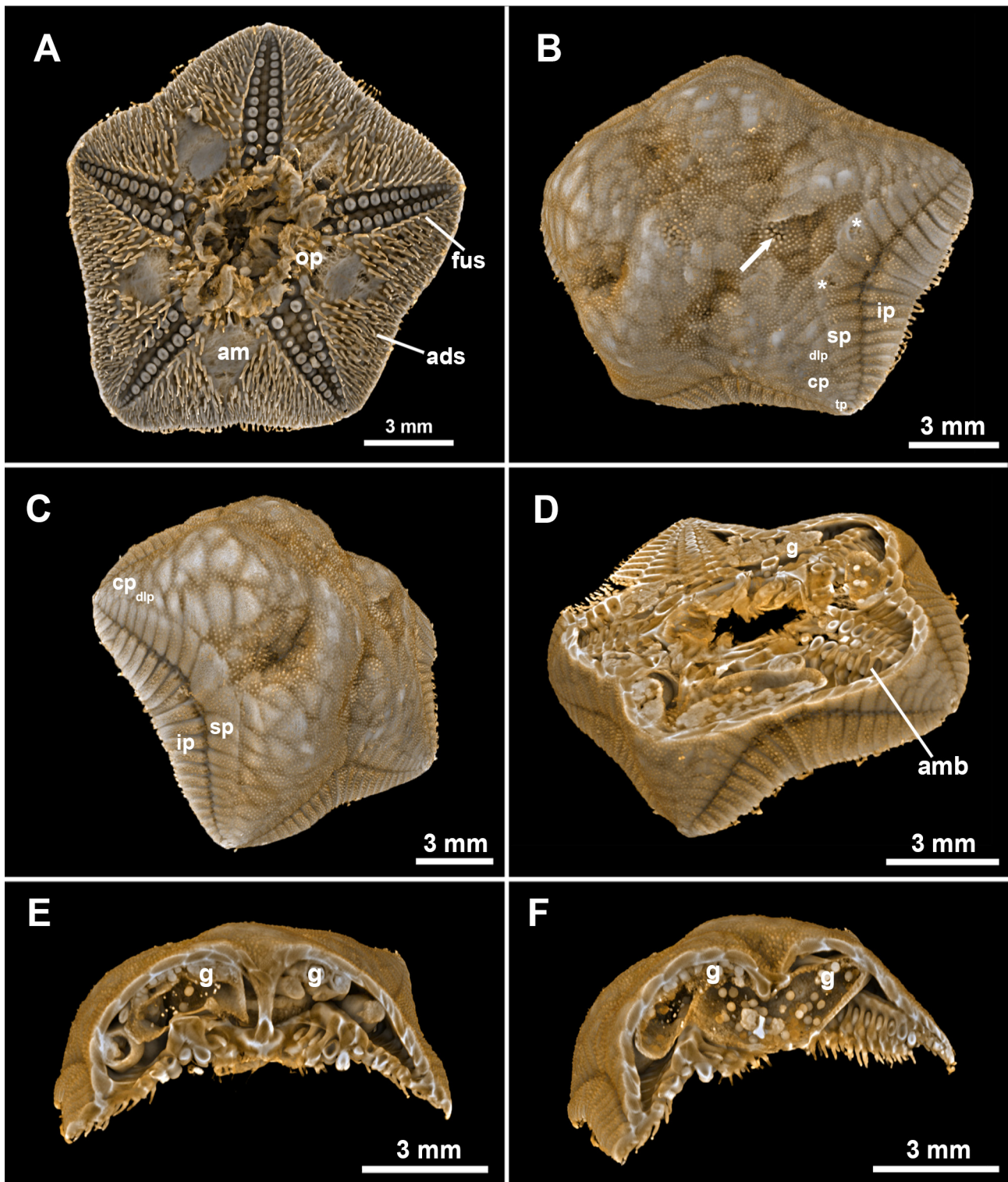
FIGURE 15. Compiled micro-CT scans of a paratype (SMF 6940) of *Caymanostella loresae* **sp. nov.** A—actinal view; B—abactinal view, with arrow indicating madreporite, *indicating gonopores; C—abactinal lateral view; D—abactinal internal view; E—cross section showing internal view of interradial chamber; F—cross section showing internal view of interradial chamber. Abbreviations: am, actinal membrane; ads, adambulacral spines; amb, ambulacral plate; cp, carinal plate; dlp, distal-lateral plate; fus, furrow spines; g, gonads; ip, inferomarginal plate; mos, marginal oral spines; op, oral plate; sp, superomarginal plate; tp, terminal plate.
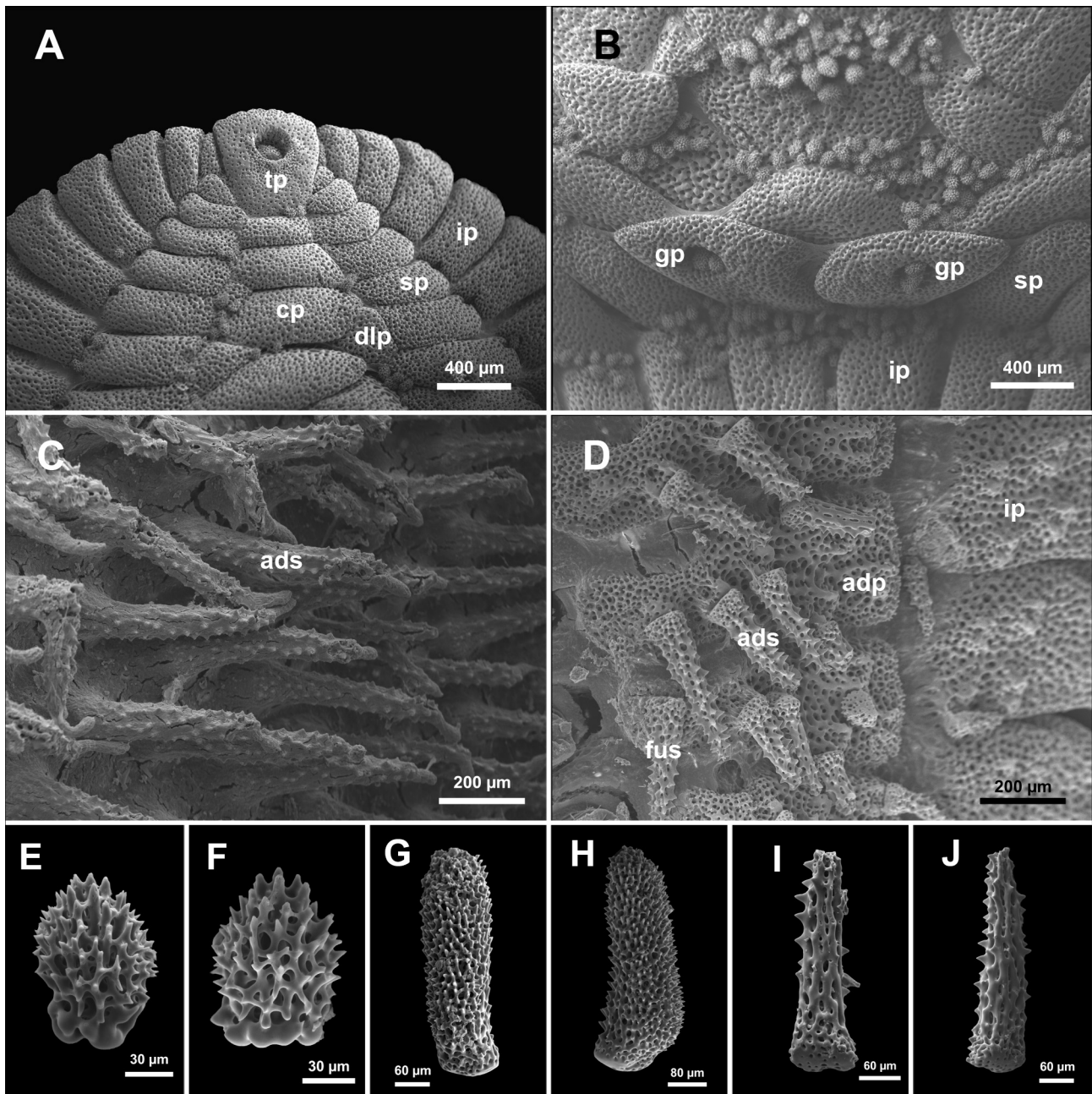
FIGURE 16. Scanning Electron Microscopy (SEM) images of *Caymanostella loresae* **sp. nov.** A—detail of bleached abactinal arm tip (paratype SIO-BIC E11393B); B—detail of bleached abactinal interradius (paratype SIO-BIC E11393B); C—detail of adambulacral spinelets on actinal side (paratype SIO-BIC E11393D); D—detail of bleached adambulacral spinelets on actinal side (paratype SIO-BIC E11393B); E, F—abactinal granule (paratype SIO-BIC E11393B); G—fringe spine, H—lateral view of fringe spine (paratype SIO-BIC E11393B); I—adambulacral spine, J—lateral view of adambulacral spine (paratype SIO-BIC E11393B). Abbreviations: adp, adambulacral plate; ads, adambulacral spines; cp, carinal plate; dlp, distal-lateral plate; fus, furrow spine; gp, gonopore; ip, inferomarginal plate; sp, superomarginal plate; tp, terminal plate.

Remarks. The pentagonal body shape of *Caymanostella loresae* **sp. nov.** differs from that of *C. scrippscognaticausa* **sp. nov.** and *C. davidalani* **sp. nov.** The shape and pattern of imbricating central disc plates also distinguishes *C. loresae* **sp. nov.** from other species in *Caymanostella* (Table 6). Terminal plates are more trapezoidal than those of *C. scrippscognaticausa* **sp. nov.** and *C. davidalani* **sp. nov.** (Fig. 16A). Inferomarginal plates are elongated, but not as much as those of *Belyaevostella* (Rowe 1989; Fujita *et al.* 1994). As in *C. admiranda* and *C. phorcynis*, the gonopores of *C. loresae* **sp. nov.** pierce through the proximal-most superomarginal plates (Table 6). Abactinal granules are like

those of *C. admiranda* in having dome-shaped crowns, yet are also narrower, exhibit a more prominent base, and have thorns that are less sharp (Table 6; Dilman *et al.* 2022). Fringe spines of *C. loresae* **sp. nov.** are also most like those of *C. admiranda*, both exhibiting dense small pores and small thorns (Table 6). Because of the thick epidermis, the actinal side appears fleshier (Fig. 13B) and takes longer to dissolve in bleach compared to adult specimens of *C. scrippscognaticausa* **sp. nov.** and *C. davidalani* **sp. nov.** When bleached, the adambulacral spines appear less tapering and elongate than those in *C. scrippscognaticausa* **sp. nov.** and *C. davidalani* **sp. nov.** (Table 6). Future work is required to compare the thick epidermis of *C. loresae* **sp. nov.** to that of *Belyaevostella* and their phylogenetic relationship involving molecular data. *Caymanostella loresae* **sp. nov.** was recovered as the sister to a clade consisted of *C.* cf. *spinimarginata*, *C. davidalani* **sp. nov.**, *C. scrippscognaticausa* **sp. nov.** and *C. laguardai* with high support (Fig. 3), with a minimum of 14.3% divergence from this sister clade in COI (Table 3, excluding *C. laguardai*, for which there is no COI data). The uncorrected 16S distance between *C. loresae* **sp. nov.** and *C. laguardai* was 14.6% (Table 4).

Etymology. *Caymanostella loresae* **sp. nov.** is named for Lores López Gómez in recognition of her unwavering commitment to advancing gender equality and her compassionate sense of justice.

4. Discussion

4.1 Taxonomic assignment of the new species

The three new species described in this study expand the known distribution of Caymanostellidae to the eastern Pacific Ocean (Fig. 1). They also include the first report of this family, including juvenile specimens, from wood falls occurring near methane seeps (Fig. 1B). Phylogenetic analyses (Fig. 3) agree with previous studies (Dilman *et al.* 2022; Janies *et al.* 2011; Mah & Blake 2012; Martin-Cao-Romero *et al.* 2021) regarding the distant relationship between *Xyloplax* and Caymanostellidae, as well as the placement of *Xyloplax* within Velatida and Caymanostellidae within Valvatida. The monophyly of terminals of Caymanostellidae was confirmed and recovered with strong support, except for a Histone H3 sequence of *Caymanostella* (GenBank EU707760; *Caymanostella* sp. MNHNP EcAs 12356 New Caledonia) which resolved instead as the sister lineage to all sampled valvatids. We interpret this result as the likely consequence of a misidentification.

The only available sequence of *C. spinimarginata* ("*Caymanostella spinimarginata*" Taiwan) was obtained from a specimen collected in the West Pacific, and no data exists for the type locality of this species in the Caribbean Sea (Table 1; Fig. 1A). Without a comparison to data of *C. spinimarginata* from the type locality, we cannot be certain about the identity of this specimen. For the same reason, the taxonomic assignment of the other publicly available *Caymanostella* sequences used in this study (Table 1) remains uncertain since none are from type localities. Due to this uncertainty, the taxonomic assignment of the new species to *Caymanostella* rather than to *Crinitostella* is rendered ambiguous to some extent, given that *C. laguardai* was recovered amongst *Caymanostella* terminals, as sister group to *C. scrippscognaticausa* **sp. nov.** (Fig. 3). We support the inclusion of the new species within *Caymanostella* due to the presence of conspicuous gonopores which are morphologically like those in other species of the genus (Dilman *et al.* 2022; Rowe 1989).

4.2 Synonymy of *Crinitostella*

Our results (Fig. 3B) suggest that *Crinitostella* should be treated as a subjective junior synonym of *Caymanostella* since it is phylogenetically nested within known representatives of *Caymanostella* (although note the caveats raised above). Additionally, diagnostic features of *Crinitostella* may also be present in *Caymanostella* and can even vary between specimens of the same *Caymanostella* species.

One of the main differences reported between *Crinitostella* and *Caymanostella* is the spiniform abactinal armament (Martin-Cao-Romero *et al.* 2021). However, this armament is variable within *Caymanostella*: that of *C. spinimarginata* and *C.* cf. *spinimarginata* consists of spinelets with a wide base, short stem, and expanded crown (Dilman *et al.* 2022; Table 6); in *C. admiranda* and *C. phorcynis,* the armament is dome-shaped (Dilman *et al.* 2022; Rowe 1989; Table 6); while the granules of *C. madagascarensis* are spherical (Dilman *et al.* 2022; Table 6). The abactinal spinelets of *Crinitostella* likely represent yet another state of an already widely variable character. Similarly,

there are multiple variations in the shape and patterns of central disc plates among species of *Caymanostella* (Table 6), suggesting that the reported differences between the abactinal plates of *Crinitostella* and *Caymanostella* (Martin-Cao-Romero *et al.* 2021) are not consistent. Although *Crinitostella* was described as lacking conspicuous gonopores in fully mature specimens, which was one of the main characters used to distinguish it from *Caymanostella* and *Belyaevostella*, *Caymanostella madagascarensis* was also described as lacking visible gonopores, inconsistent with the reported differences between *Crinitostella* and *Caymanostella* (Martin-Cao-Romero *et al.* 2021; Dilman *et al.* 2022; Table 6).

Morphological analysis of *C. scrippscognaticausa* **sp. nov.** and *C. davidalani* **sp. nov.**, including specimens at various life stages, showed that a wide variety of other morphological characteristics can potentially be related to ontogeny (see Variation). For example, the slit-like madreporite shape described for *C. spinimarginata* is also seen in intermediate-sized specimens of *C. scrippscognaticausa* **sp. nov.** (e.g., SMF 6939, Fig. 6A, C and E11221B) and *C. davidalani* **sp. nov.** (MZUCR ECH2403, Fig. 11E). Small specimens of *C. scrippscognaticausa* **sp. nov.**, such as SMF 6938 (Fig. 7), have abactinal plate shapes and patterns like small species within the genus, such as *C. admiranda* and *C. madagascarensis*. *Crinitostella* is like some *Caymanostella* in having a well-defined longitudinal row of carinal plates (Martin-Cao-Romero *et al.* 2021), but not all *Caymanostella* species have discernable carinal rows according to Dilman *et al.* (2022) (Table 6). This character could also potentially vary with ontogeny, as smaller specimens tend to have fewer plates on the arms, thus making the carinal row more discernible, as seen in *C. scrippscognaticausa* **sp. nov.** (SMF 6938, Fig. 7A, C), *C. admiranda* and *C. madagascarensis* (Dilman *et al.* 2022; Table 6). Distal-lateral plates, on the other hand, could appear absent in small specimens due to low number of plates on the arm (Fig. 7A, C).

In summary, *Crinitostella* was erected based on diagnostic characters already widely variable within *Caymanostella*, and that are shown here to exhibit intraspecific and ontogenetic variability as well. Based on this variation and the current phylogenetic placement of *Crinitostella* within *Caymanostella* sequenced to date (Fig. 3) we formally synonymize *Crinitostella* with *Caymanostella* and refer to *Crinitostella laguardai* as *Caymanostella laguardai* n. comb. Molecular data for the remaining *Caymanostella* species, especially *C. spinimarginata* from its type locality (Cayman Trench), may warrant further taxonomic revisions.

4.3 Ecology

Caymanostellids are considered obligate wood-fall dwellers, an interpretation supported not only by their sampling records, but also by their highly specialized morphology. This includes a flattened body shape and broad oral opening that maximizes contact with the substrate, as well as actinal spines which potentially assist in anchoring on wood substrates (Dilman *et al.* 2022). However, little is known about their diet and life history due to the limited number of specimen records and the overall difficulty of observing and collecting them. Belyaev (1974) suggested that Caymanostellidae could be predators, feeding on other animals dwelling on sunken wood. Wolff (1979) analyzed the gut content of *Caymanostella spinimarginata* specimens and concluded that they might feed on wood, wood-associated microorganisms, or both. No specimens other than those analyzed by Wolff (1979) have been reported to contain wood fragments or other food particles in their mouth or stomach. Dilman *et al.* (2022) noted the lack of evidence of wood-digestion mechanisms (such as gut symbiotic bacteria) and were unable to find wood feeding traces at the collection sites of specimens they called *Caymanostella* cf. *spinimarginata*. Stable isotope analysis on preserved specimens might provide a more accurate assessment of their ecological niche, providing better clues on their diet and role in wood fall communities. Because of the relatively small size and deep distribution of caymanostellids, *in-situ* observation may not currently be practical for studying the feeding ecology of these organisms. Additionally, caymanostellids likely use the typical feeding strategy of sea stars by everting their stomachs and digesting food outside their body. Therefore, other environmental substances in addition to food particles may show up in their gut contents.

Wood colonization experiments can provide ecological information on life history and dispersal routes, as well as enable the discovery of new species and range expansions (Mah 2006; Romano *et al.* 2020). Besides caymanostellids, recent experimental deployments near methane seeps at the Pacific margin of Costa Rica have yielded new species of sea stars (Payne *et al.* 2023), ribbon worms (Sagorny *et al.* 2022), and scale worms (Hatch *et al.* 2020). It is not uncommon for benthic invertebrates to occur on multiple types of substrates. Notably, the occurrence of *Xyloplax*

princealberti Payne, Tilic, Boschen-Rose, Gannon, Stiller, Hiley, Grupe, Mah & Rouse, 2023 on *Ridgeia piscesae* Jones, 1985 tubeworms at the Juan de Fuca Ridge, Canada, represents the first record of *Xyloplax* from non-wood substrates (Payne *et al.* 2023). *Peinaleopolynoe* Desbruyères & Laubier, 1988 scale worms occur on organic falls, seeps and hydrothermal vents. Based on phylogenetic evidence, it is likely that *Peinaleopolynoe* species that occur on seeps and vents evolved through secondary colonizations from organic falls (Hatch *et al.* 2020). This correlates with the "steppingstone" hypothesis suggested from community composition analysis of deployed substrates near the Costa Rica methane seep at Mound 12 by Pereira *et al.* (2022). As previously suggested (Bernardino *et al.* 2012; Bienhold *et al.* 2013; Distel *et al.* 2000; Pop Ristova *et al.* 2017), this hypothesis implies that organic substrates harboring chemosynthetic communities can facilitate colonization and connection between various chemosynthetic habitats, including vents and seeps. Therefore, future wood deployment experiments could provide further information to understand the life history of Caymanostellidae and other woodfall-associated organisms, as well as their diversity and connectivity across depth and geographical space, improving our understanding of the evolutionary history of these unique ecosystems.

References

Altschul, S.F., Gish, W., Miller, W., Myers, E.W. & Lipman, D.J. (1990) Basic local alignment search tool. *Journal of Molecular Biology*, 215, 403–410.
https://doi.org/10.1016/S0022-2836(05)80360-2

Alvarado, J.J., Chacón-Monge, J.L., Azofeifa-Solano, J.C. & Cortés, J. (2022) Diversity of deep-sea echinoderms from Costa Rica. *Frontiers in Marine Science*, 9, 918878.
https://doi.org/10.3389/fmars.2022.918878

Arndt, A., Marquez, C., Lambert, P. & Smith, M.J. (1996) Molecular phylogeny of eastern Pacific sea cucumbers (Echinodermata: Holothuroidea) based on mitochondrial DNA sequence. *Molecular Phylogenetics and Evolution*, 6, 425–437.
https://doi.org/10.1006/mpev.1996.0091

Aziz, A. & Jangoux, M. (1984) Description de quatre nouvelles espèces d'astérides profonds (Echinodermata) de la région Indo-Malaise. *Indo-Malayan Zoology*, 1, 187–194.

Baker, A.N., Rowe, F.W.E. & Clark, H.E.S. (1986) A new class of Echinodermata from New Zealand. *Nature*, 321, 862–864.
https://doi.org/10.1038/321862a0

Barroso, R., Kudenov, J.D., Halanych, K.M., Saeedi, H., Sumida, P.Y.G. & Bernardino, A.F. (2018) A new species of xylophilic fireworm (Annelida: Amphinomidae: *Cryptonome*) from deep-sea wood falls in the SW Atlantic. *Deep Sea Research Part I: Oceanographic Research Papers*, 137, 66–75.
https://doi.org/10.1016/j.dsr.2018.05.005

Becker, P., Samadi, S., Zbinden, M., Hoyoux, C., Compère, P. & De Ridder, C. (2009) First insights into the gut microflora associated with an echinoid from wood falls environments. *Cahiers de Biologie Marine*, 50, 343–352.

Belyaev, G.M. (1974) A new family of abyssal starfishes. *Zoologischeskii Zhurnal*, 53, 1502–1508.

Belyaev, G.M. (1990) Is it valid to isolate the genus *Xyloplax* as an independent class of echinoderms? *Zoologicheskii Zhurnal*, 69, 83–96.

Bernardino, A.F., Levin, L.A., Thurber, A.R. & Smith, C.R. (2012) Comparative composition, diversity and trophic ecology of sediment macrofauna at vents, seeps and organic falls. *PLoS ONE*, 7, e33515.
https://doi.org/10.1371/journal.pone.0033515

Bienhold, C., Pop Ristova, P., Wenzhöfer, F., Dittmar, T. & Boetius, A. (2013) How deep-sea wood falls sustain chemosynthetic life. *PLoS ONE*, 8, e53590.
https://doi.org/10.1371/journal.pone.0053590

Blake, D.B. (1987) A classification and phylogeny of post-Palaeozoic sea stars (Asteroidea: Echinodermata). *Journal of Natural History*, 21, 481–528.
https://doi.org/10.1080/00222938700771141

Brett, C.H. (2017) Evolutionary biology of wood-eating sea urchins (Temnopleuridea: Trigonocidaridae). Master of Science Thesis, San Francisco State University. Available from: http://hdl.handle.net/10211.3/199487 (accessed 7 October 2024)

Clement, M., Posada, D. & Crandall, K.A. (2000) TCS: a computer program to estimate gene genealogies. *Molecular Ecology*, 9, 1657–1659.
https://doi.org/10.1046/j.1365-294x.2000.01020.x

Colgan, D.J., Ponder, W.F., Beacham, E., & Macaranas, J. (2003) Gastropod phylogeny based on six segments from four genes representing coding or non-coding and mitochondrial or nuclear DNA. *Molluscan Research*, 23, 123–148.
https://doi.org/10.1071/MR03002

Darriba, D., Posada, D., Kozlov, A.M., Stamatakis, A., Morel, B. & Flouri, T. (2019) ModelTest-NG: A new and scalable tool for the selection of DNA and protein evolutionary models. *Molecular Biology and Evolution*, 37, 291–294.
https://doi.org/10.1093/molbev/msz189

Dilman, A.B., Minin, K.V. & Petrov, N.B. (2022) New record of the wood-associated sea star *Caymanostella*, with notes on the phylogenetic position of the family Caymanostellidae (Asteroidea). *Zoological Journal of the Linnean Society*, 194, 14–35.
https://doi.org/10.1093/zoolinnean/zlab060

Distel, D.L., Baco, A.R., Chuang, E., Morrill, W., Cavanaugh, C. & Smith, C.R. (2000) Do mussels take wooden steps to deep-sea vents? *Nature*, 403, 725–726.
https://doi.org/10.1038/35001667

Duperron, S., Lorion, J., Samadi, S., Gros, O. & Gaill, F. (2009) Symbioses between deep-sea mussels (Mytilidae: Bathymodiolinae) and chemosynthetic bacteria: diversity, function and evolution. *Comptes Rendus Biologies*, 332, 298–310.
https://doi.org/10.1016/j.crvi.2008.08.003

Edler, D., Klein, J., Antonelli, A. & Silvestro, D. (2021) raxmlGUI 2.0: A graphical interface and toolkit for phylogenetic analyses using RAxML. *Methods in Ecology and Evolution*, 12, 373–377.
https://doi.org/10.1111/2041-210X.13512.

Fujita, T., Stampanato, S. & Jangoux, M. (1994) *Beyaevostella hyugaenis*: a new species of deep-sea asteroid (Asteroidea, Caymanostellidae) found on a sunken wood from off southern Japan. *Bulletin of the National Science Museum, Tokyo*, 20, 183–188.

Gale, A.S. (2011) The phylogeny of post-palaeozoic Asteroidea (Neoasteroidea, Echinodermata). *Special Papers in Palaeontology*, 85, 1–112.

Hatch, A.S., Liew, H., Hourdez, S. & Rouse, G.W. (2020) Hungry scale worms: Phylogenetics of *Peinaleopolynoe* (Polynoidae, Annelida), with four new species. *ZooKeys*, 932, 27–74.
https://doi.org/10.3897/zookeys.932.48532

Hookabe, N., Moritaki, T., Jimi, N. & Ueshima, R. (2022) A new oerstediid discovered from wood falls in the Sea of Kumano, Japan: Description of *Rhombonemertes rublinea* gen. et sp. nov. (Nemertea: Eumonostilifera). *Zoologischer Anzeiger*, 301, 154–162.
https://doi.org/10.1016/j.jcz.2022.10.003

Janies, D.A., Voight, J.R. & Daly, M. (2011) Echinoderm phylogeny including *Xyloplax*, a progenetic asteroid. *Systematic Biology*, 60, 420–438.
https://doi.org/10.1093/sysbio/syr044

Katoh, K. & Standley, D.M. (2013) MAFFT Multiple Sequence Alignment Software Version 7: Improvements in performance and usability. *Molecular Biology and Evolution*, 30, 772–780.
https://doi.org/10.1093/molbev/mst010

Kozlov, A.M., Darriba, D., Flouri, T., Morel, B. & Stamatakis, A. (2019) RAxML-NG: a fast, scalable and user-friendly tool for maximum likelihood phylogenetic inference. *Bioinformatics*, 35, 4453–4455.
https://doi.org/10.1093/bioinformatics/btz305

Leigh, J.W. & Bryant, D. (2015) PopART: Full-feature software for haplotype network construction. *Methods in Ecology and Evolution/British Ecological Society*, 6, 1110–1116.
https://doi.org/10.1111/2041-210x.12410

Limaye, A. (2012) Drishti: a volume exploration and presentation tool. In: *Developments in X-Ray Tomography VIII*. SPIE, Bellingham, Washington, pp. 191–199.

https://doi.org/10.1117/12.935640

Linchangco, G.V., Foltz, D.W., Reid, R., Williams, J., Nodzak, C., Kerr, A.M., Miller, A.K., Hunter, R., Wilson, N.G., Nielsen, W.J., Mah, C.L., Rouse, G.W., Wray, G.A. & Janies, D.A. (2017) The phylogeny of extant starfish (Asteroidea: Echinodermata) including *Xyloplax*, based on comparative transcriptomics. *Molecular Phylogenetics and Evolution*, 115, 161–170.
https://doi.org/10.1016/j.ympev.2017.07.022

Maddison, W.P. & Maddison, D.R. (2023) *Mesquite: a modular system for evolutionary analysis. Version 3.70.* Available from: http://www.mesquiteproject.org (accessed 27 June 2023)

Magalhães, W.F., Linse, K. & Wiklund, H. (2017) A new species of *Raricirrus* (Annelida: Cirratuliformia) from deep-water sunken wood off California. *Zootaxa*, 4353 (1), 51–68.
https://doi.org/10.11646/zootaxa.4353.1.3

Magalhães, W.F. & Hilliard, J. (2022) Two new deep-sea species of *Capitella* (Annelida: Capitellidae) from sunken wood in the Northeast Pacific. *Zootaxa*, 5125 (2), 229–240.
https://doi.org/10.11646/zootaxa.5125.2.7

Mah, C.L. (2006) A new species of *Xyloplax* (Echinodermata: Asteroidea: Concentricycloidea) from the northeast Pacific: comparative morphology and a reassessment of phylogeny. *Invertebrate Biology*, 125, 136–153.
https://doi.org/10.1111/j.1744-7410.2006.00048.x

Mah, C.L. & Blake, D.B. (2012) Global diversity and phylogeny of the Asteroidea (Echinodermata). *PLoS ONE*, 7, e35644.
https://doi.org/10.1371/journal.pone.0035644

Martin-Cao-Romero, C., Solís-Marín, F.A. & Bribiesca-Contreras, G. (2021) *Crinitostella laguardai*, new genus and species of wood-dwelling deep-sea sea-star (Asteroidea: Caymanostellidae) from the Gulf of Mexico. *Journal of the Marine Biological Association of the United Kingdom*, 101, 591–597.
https://doi.org/10.1017/S0025315421000448

Okanishi, M., Kato, M., Watanabe, H.K., Chen, C. & Fujita, T. (2020) Large populations of two new species of *Ophiambix* (Echinodermata, Ophiuroidea) discovered on Japanese hot vents and cold seeps. *Raffles Bulletin of Zoology*, 68, 196–213.
https://doi.org/10.26107/RBZ-2020-0017

Palumbi, S.R. (1996) Nucleic acids II: the polymerase chain reaction. *In*: Hillis, D.M., Moritz, G. & Mable, B.K. (Eds.), *Molecular Systematics. 2nd Edition*. Sinauer, Sunderland, Massachusetts, pp. 205–247.

Payne, C.Y., Tilic, E., Boschen-Rose, R.E., Gannon, A., Stiller, J., Hiley, A.S., Grupe, B.M., Mah, C.L. & Rouse, G.W. (2023) *Xyloplax princealberti* (Asteroidea, Echinodermata): A new species that is not always associated with wood falls. *Diversity*, 15, 1212.
https://doi.org/10.3390/d15121212

Pereira, O.S., Gonzalez, J., Mendoza, G., Le, J., McNeill, M., Ontiveros, J., Lee, R.W., Rouse, G.W., Cortés, J. & Levin, L.A. (2022) Does substrate matter in the deep sea? A comparison of bone, wood, and carbonate rock colonizers. *PLoS ONE*, 17, e0271635.
https://doi.org/10.1371/journal.pone.0271635

Pop Ristova, P., Bienhold, C., Wenzhöfer, F., Rossel, P.E. & Boetius, A. (2017) Temporal and spatial variations of bacterial and faunal communities associated with deep-sea wood falls. *PLoS ONE*, 12, e0169906.
https://doi.org/10.1371/journal.pone.0169906

Romano, C., Nunes-Jorge, A., Le Bris, N., Rouse, G.W., Martin, D. & Borowski, C. (2020) Wooden stepping stones: Diversity and biogeography of deep-sea wood boring Xylophagaidae (Mollusca: Bivalvia) in the North-East Atlantic Ocean, with the description of a new genus. *Frontiers in Marine Science*, 7.
https://doi.org/10.3389/fmars.2020.579959

Rowe, F.W.E. (1988) Review of the extant class Concentricycloidea and reinterpretation of the fossil class Cyclocystoidea. *In*: Burke, R.D., Mladenov, P.V., Lambert, P. & Parsley, R.L. (Eds.), *Echinoderm Biology*. Balkema, Rotterdam, pp. 3–15.

Rowe, F.W.E. (1989) A review of the family Caymanostellidae (Echinodermata: Asteroidea) with the description of a new species of *Caymanostella* Belyaev and a new genus. *Proceedings of the Linnean Society of New South Wales. Linnean Society of New South Wales*, 111, 293–307.

Saeedi, H., Bernardino, A.F., Shimabukuro, M., Falchetto, G. & Sumida, P.Y.G. (2019) Macrofaunal community structure and biodiversity patterns based on a wood-fall experiment in the deep South-west Atlantic. *Deep Sea Research*, Part I: Oceanographic Research Papers, 145, 73–82.
https://doi.org/10.1016/j.dsr.2019.01.008

Sagorny, C., von Döhren, J., Rouse, G.W. & Tilic, E. (2022) Cutting the ribbon: bathyal Nemertea from seeps along the Costa Rica margin, with descriptions of 2 new genera and 9 new species. *European Journal of Taxonomy*, 845, 132–174.
https://doi.org/10.5852/ejt.2022.845.1959

Smith, A.B. (1988) To group or not to group: the taxonomic position of *Xyloplax*. *In*: Burke, R.D., Mladenov, P.V., Lambert, P. & Parsley, R.L. (Eds.), *Echinoderm Biology: Proceedings of the Sixth International Echinoderm Conference.* Balkema, Rotterdam, pp. 17–23.

Smith, C.R., Glover, A.G., Treude, T., Higgs, N.D. & Amon, D.J. (2015) Whale-fall ecosystems: recent insights into ecology, paleoecology, and evolution. *Annual review of marine science* 7, 571–596.
https://doi.org/10.1146/annurev-marine-010213-135144

Swofford, D.L. (2002) *PAUP* Phylogenetic Analysis Using Parsimony (and other methods)*. Available from: https://paup.phylosolutions.com (accessed 3 May 2024)

Tandberg, A.H.S., Rapp, H.T., Schander, C. & Vader, W. (2013) A new species of *Exitomelita* (Amphipoda: Melitidae) from a deep-water wood fall in the northern Norwegian Sea. *Journal of natural history*, 47, 1875–1889.
https://doi.org/10.1080/00222933.2012.725778

Vaidya, G., Lohman, D.J. & Meier, R. (2011) SequenceMatrix: concatenation software for the fast assembly of multi-gene datasets with character set and codon information. *Cladistics: the international journal of the Willi Hennig Society*, 27, 171–180.
https://doi.org/10.1111/j.1096-0031.2010.00329.x.

Voight, J.R. (2015) Xylotrophic bivalves: aspects of their biology and the impacts of humans. *The Journal of molluscan studies*, 81, 175–186.
https://doi.org/10.1093/mollus/eyv008

Voight, J.R., Marshall, B.A., Judge, J., Halanych, K.M., Li, Y., Bernardino, A.F., Grewe, F. & Maddox, J.D. (2019) Life in wood: preliminary phylogeny of deep-sea wood-boring bivalves (Xylophagaidae), with descriptions of three new genera and one new species. *The Journal of molluscan studies*, 85, 232–243.
https://doi.org/10.1093/mollus/eyz003

Wolff, T. (1979) Macrofaunal utilization of plant remains in the deep sea. *Sarsia*, 64, 117–143.
https://doi.org/10.1080/00364827.1979.10411373